ACS APPLIED MATERIALS & INTERFACES

Research Article

www.acsami.org

Acute *in Vivo* Toxicity Mitigation of PEI-Coated Maghemite Nanoparticles Using Controlled Oxidation and Surface Modifications toward siRNA Delivery

Liron Limor Israel,[†,§,∥] Emmanuel Lellouche,[‡,§,∥] Stella Ostrovsky,[†,§] Valeria Yarmiayev,[†,§] Moshe Bechor,[‡,§] Shulamit Michaeli,*[,‡,§] and Jean-Paul (Moshe) Lellouche*[,†,§]

[†]Department of Chemistry, [‡]Faculty of Life Sciences, and [§]Institute of Nanotechnology & Advanced Materials, Bar-Ilan University, Ramat-Gan, 5290002, Israel

Supporting Information

ABSTRACT: A ceric ammonium nitrate (CAN)-based doping step was used for the fabrication of core maghemite nanoparticles (NPs) that enabled the obtainment of colloid particles with a view to a high-level nanoparticle (NP) surface doping by Ce(III/IV). Such doping of Ce(III/IV) cations enables one to *exploit their quite rich coordination chemistry* for ligand coordinative binding. In fact, they were shown to act as *powerful Lewis acid centers* for attaching any organic (Lewis base) ligand such as a 25 kDa branched PEI polymer. Resulting $_{con}PEI_{25}$-CAN-γ-Fe_2O_3 NPs have been fully characterized before a successful implementation of siRNA loading and cell delivery/gene silencing using a well-known dual luciferase system. This attractive result emphasized their significant potential as an NP platform technology toward additional MRI and/or drug delivery (peptide)-relating end applications. However, due to their high positive charge, PEI polymers can cause severe *in vivo* toxicity due to their interaction with negatively charged red blood cells (RBC), resulting in RBC aggregation and lysis, leading to thrombosis and, finally, to animal death. In order to mitigate these acute toxic effects, two different types of surface modifications were performed. One modification included the controlled oxidation of 0.1−5% of the PEI amines before or after conjugation to the NPs, using hydrogen peroxide or potassium persulfate. The other type of modification was the addition of a second biocompatible polyanionic polymer to the PEI grafted NPs, based on the concept of a layer-by-layer (LbL) technique. This modification is based on the coordination of another polyanionic polymer on the NPs surface in order to create a combined hybrid PEI and polyanionic polymer nanosystem. In both cases, the surface modification successfully mitigated the NP acute *in vivo* toxicity, without compromising the silencing efficiency.

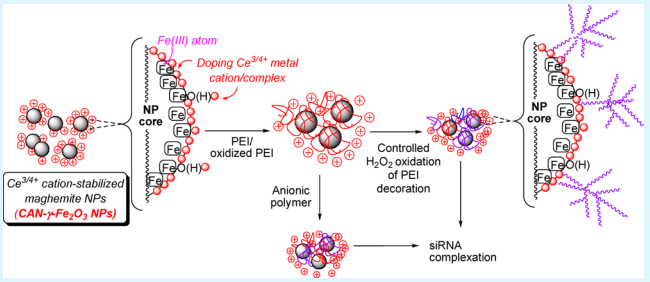

KEYWORDS: *nanoparticle-based drug delivery systems, maghemite nanoparticle surface engineering, layer-by-layer (LbL) nanoparticle surface modifications, design of experiments (DoE), PEI toxicity mitigation, PEI oxidation, siRNA delivery, gene silencing*

1. INTRODUCTION

1.1. Magnetic Inorganic Iron-Based Nanoparticles: Generalities and Their Use in Drug Delivery. Both magnetically responsive magnetite (Fe_3O_4)- and maghemite (γ-Fe_2O_3)-based nanoscale particles are the subject of a current intense and sustained interest from the scientific community due to their several attractive specific factors that have been summarized as follows:[1−10]

First, these crystalline spinel phases can be readily prepared as nanoscale 3.0−100.0 nm sized formulations.[1] Second, atom vacancies (surface defects) and polar amphoteric HO-decorating species enable an easy surface chemical manipulation for postnanoparticle fabrication surface engineering at the second step functionalization levels. Third, both magnetite and maghemite NPs are magnetically responsive (ferrimagnetic phases), i.e., enabling (i) magnetically targeted drug delivery systems, (ii) anticancer local hyperthermia (heat-driven cancer ablation), (iii) internal tissue imaging when used as nanoscale contrast agents (magnetic resonance imaging), and (iv) cell/ligand bioseparations. Lastly, magnetite and maghemite NPs, as well as relating dual phase iron oxide core−polymer shell nanocomposites, are generally considered as safe minimally toxic particulate systems that have been authorized for *in vivo* clinical use (MRI contrast agents).[11]

Beyond the NP surface enabling functionalization capability, as mentioned earlier, it is notable that the NP surface passivation is achieved by using small functional ligands. Some organic modes of NP decoration/passivation by *organic*

Received: March 30, 2015
Accepted: June 29, 2015
Published: June 29, 2015

DOI: 10.1021/acsami.5b02743
ACS Appl. Mater. Interfaces 2015, 7, 15240−15255

Scheme 1. Illustrative Scheme Describing the Overall Fabrication of $_{con}PEI_{25}$-CAN-γ-Fe_2O_3 NPs, the Controlled Oxidation toward $_{con}PEI_{25\text{-}ox}$-CAN-γ-Fe_2O_3 NPs, and the Controlled Oxidation and Fabrication of $_{con}PEI_{25\text{-}pp}$-CAN-γ-Fe_2O_3 NPs for RNA Loading/Gene Silencing (Cell Transfection)[a]

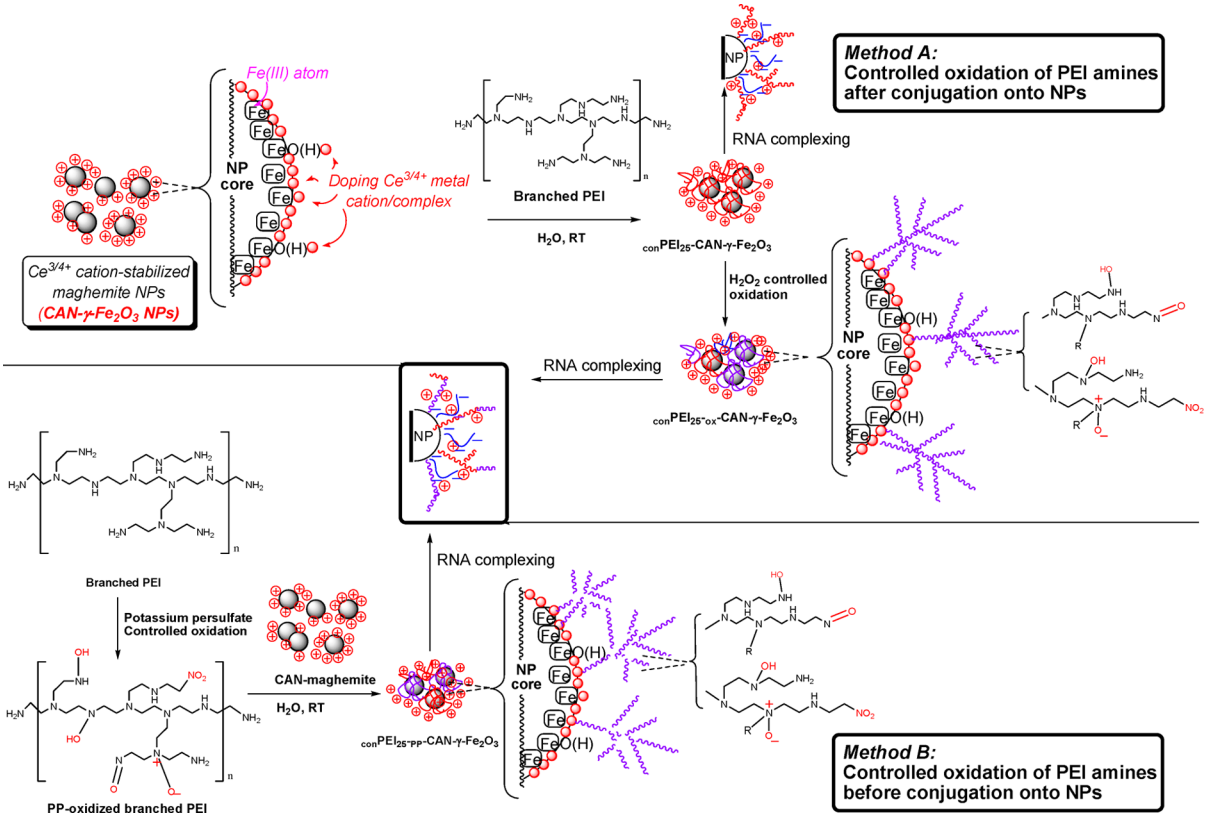

[a]The chemical modifications of *b*-PEI_{25} functions post oxidation reaction (for both A and B methods) have been presented for illustration only.

chemical species might cause (i) a deterioration of magnetic properties (saturation magnetization M_s), (ii) problems of composite toxicity, and (iii) limitations of NP concentration ranges used for safe storage and transport.

1.2. siRNA-Mediated Gene Silencing. The mechanism of gene silencing goes through inhibition of the conversion of mRNA into protein.[12] siRNAs are not naturally present in mammalian cells but can be designed to be efficiently incorporated into the RNA-induced silencing complex (RISC) and induce the degradation of any mRNA at will.[13,14]

Despite the potentially high therapeutic advantages of siRNAs, such therapies are yet unavailable in clinics, since naked and unmodified siRNAs can be degraded by endonucleases, excreted by a renal clearance, or may even cause undesirable off-target effects.[15] In addition, due to their large molecular weight (MW ~ 13 kDa), their negative charge, and their hydrophilic nature, siRNA molecules are unable to cross cell membranes by passive diffusion mechanisms. These limitations have led to the development of a wide range of nanocarriers, including cyclodextrin polymers,[16−18] lipid-based carriers,[19,20] dendrimers,[21,22] neutral and/or cationic polymers,[23,24] and conjugated siRNAs,[25,26] as well as various nanoparticle formulations.[27−29]

One of the most efficient transfecting agents for the delivery of nucleic acids, both *in vitro* and *in vivo*, makes use of polycationic polyethylenimine (PEI) polymers. PEI polymers possess a high positive charge density due to the presence of positively charged ammonium (NH_4^+) ions in aqueous media. Thus, PEI polymers have a powerful proton adsorption capacity, qualified as their intrinsic "proton sponge" effect. Since PEI contains a large quantity of variously protonatable nitrogen atoms, its protonation level most likely increases when the medium pH decreases to values around 5.0 within the endosomal/lysosomal compartments, which leads to an influx of chloride ions and, consequently, to lysosome osmotic swelling and rupture. This overall process results in an efficient release of nucleic acids from the endosome/lysosome compartments to the cytosol.[30−33]

Nevertheless, due to their high positive charge, PEI polymers can also cause severe *in vivo* toxicity due to strong interactions with negatively charged red blood cells (RBC), resulting in RBC aggregation and lysis, which leads to thrombosis, and finally, to a rapid animal death.[34,35] Different approaches have been considered to modify the original PEI polymers in order to mitigate their toxicity.[36] These modifications include the conjugation of PEI with different chemically reactive molecules, such as polysaccharides (chitosan, pullulan, and hyaluronic acid)[37−39] and hydrophobic moieties (cholesterol, cholic acid, and stearic acid),[40−42] as well as poly(ethylene glycol) polymers (PEGs).[43−45]

1.3. Magnetic Nanoscale Carriers for DNA/RNA Delivery and Cell Transfection. Iron oxide particles have many applications in biomedicine, such as in MRI, drug delivery, stem cell tracking, heat source hyperthermia, and more.[2] In particular, current advanced techniques in drug targeting use delicate surface modifications on these particles for the conjugation of antiangiogenic and anticancer drugs.[46] Numerous iron oxide NPs are already FDA-approved and

DOI: 10.1021/acsami.5b02743
ACS Appl. Mater. Interfaces 2015, 7, 15240−15255

Scheme 2. Illustrative Scheme Describing the LbL-Based Polyanionic Polymer Modification Executed onto the Surface of $_{con}PEI_{25}$-CAN-γ-Fe_2O_3 NPs

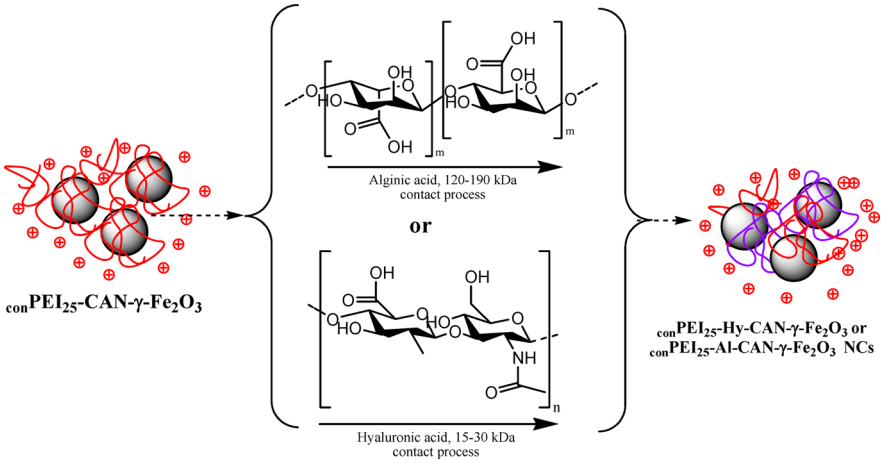

several more are undergoing clinical trials.[2] A previous work has summarized many *in vitro* and *in vivo* features of different iron oxide based particles that are functionalized by a variety of polymers.[47] Most of these studies utilize liposomes, dendrimers, and polymer particles, for both *in vitro* and *in vivo* siRNA delivery into cells. NPs can penetrate tumor cells by the enhanced permeability and retention effect (EPR), but specific localization, as well as an enhanced internalization, has also been demonstrated, upon the binding of specific targeting moieties such as antibodies, transferrin, folic acid, and aptamers onto NPs.[46,48−51]

1.4. Super-paramagnetic $Ce^{3+/4+}$-Doped Maghemite (γ-Fe_2O_3) and PEI-$Ce^{3+/4+}$-Doped Maghemite Nanoparticles for DNA/RNA Delivery and Cell Transfection. Previous works that have recently been published in a preliminary form[52] have already established that all known *organic* and *inorganic* modes of aggregation control/surface functionalization of iron oxide (magnetite and maghemite) NPs can be readily bypassed by using an ultrasound-assisted oxidative process involving the strong monoelectronic oxidant ceric ammonium nitrate [CAN, $Ce^{IV}(NH_4)_2(NO_3)_6$].[53−55] Indeed, the high-power ultrasonication readily afforded non-aggregated super-paramagnetic $Ce^{3+/4+}$ metal cation-doped maghemite (γ-Fe_2O_3) NPs (CAN-γ-Fe_2O_3 NPs; Scheme 1). In this context, a more recent work[56,57] described *a modified and improved experimental $Ce^{3+/4+}$doping process* on the surface of the same preformed MASSART[58] magnetite (a global optimization by DoE method), which resulted in (i) a much higher and consistent level of $Ce^{3+/4+}$ cation surface doping and (ii) the discovery that doping $Ce^{3+/4+}$ cations within corresponding [$Ce^{3+/4+}L_n$] complexes might act as "hard" Lewis acid centers in order to exploit *the known rich [$Ce^{3+/4+}$]-complex ligand coordination chemistry*.[59−63] This improved doping process *(a new doping process)* was made quantitatively significant *relating to the amount of doping $Ce^{3+/4+}$ cations/ [$Ce^{3+/4+}L_n$] complexes* that resulted in an innovative way to bind *any Lewis-base-containing species* (N/O/S-heteroatom-containing organic moieties) for an NP decoration/functionalization. As a matter of consequence, such [$Ce^{3+/4+}L_n$] complex-doped maghemite (γ-Fe_2O_3) NPs were successfully modified by a typical contacting polycationic 25 kDa *b*-PEI polymer.[56] In order to reduce the known *in vivo* toxicity often associated with PEI, new surface modifications were considered. In previous studies, various attempts to reduce the PEI toxicity by generating a number of nontoxic derivates of branched PEI, through the modification of amines by ethyl acrylate, acetylation of primary amines, or introduction of negatively charged propionic or succinic acid groups in the polymer structure,[64] or by PEGylation,[65] were made. A more recent publication describes a reduction in free PEI toxicity by using oxidation as a facile strategy, in order to reduce its surface charge.[66] Nevertheless and in the present study as detailed later, controlled PEI oxidation reactions do not reduce NPs' surface charge when using a significant molar amount of aqueous $H_2O_2/K_2S_2O_8$, but rather increase it even when using very small molar amounts of aqueous $H_2O_2/K_2S_2O_8$. This phenomenon of NPs toxicity mitigation likely arises from PEI-coordinating features of the $Ce^{3+/4+}$ metal cation shell as an active influential factor.

As cited earlier, one such chemical modification that we decided to use involves the controlled oxidation of PEI aminated functions, either *after (method A) or before (method B)* the attachment of the polymer onto the NP surface, by using either H_2O_2 or $K_2S_2O_8$ (potassium persulfate, PP) (Scheme 1). Such chemical modifications may strongly decrease the NPs' acute toxicity, probably because of the corresponding decrease of the number of PEI reactive primary amines.[66] An oxidation of both secondary and tertiary amines can also occur, but since the primary amines are more reactive, it is likely that these will react first. Primary amines can be oxidized into hydroxyl amines which should be less toxic than the primary amines.

Another possible modification of a different kind includes the addition of a second biocompatible polyanionic polymer onto the $_{con}PEI_{25}$-CAN-γ-Fe_2O_3 NPs in a manner similar to method A (Scheme 2). This modification is based on the coordination of another polyanionic polymer on the $_{con}PEI_{25}$-CAN-γ-Fe_2O_3 surface, in order to create a combined hybrid PEI polyanionic polymer nanosystem. These NPs were prepared based on the concept of a layer-by-layer (LbL) outer shell modification/ formation when using formerly fabricated $_{con}PEI_{25}$-CAN-γ-Fe_2O_3 NPs. Two types of polyanionic polymers showed potential: alginic (Al) and hyaluronic (Hy) acids.

Furthermore, a combination of the two types of modifications was executed in order to reduce the toxicity even further: The LbL modification, using alginic acid, was performed on oxidized $_{con}PEI_{25\text{-}ox}$-CAN-γ-Fe_2O_3 NPs.

DOI: 10.1021/acsami.5b02743
ACS Appl. Mater. Interfaces 2015, 7, 15240−15255

Table 1. Summary of Nanosystem Characterization Using DLS, Size Distribution by TEM, and ζ Potential

NP type	hydrodynamic diam (nm)	size distribution by TEM (nm)	ζ potential (mV)
$_{con}PEI_{25}$-γ-Fe_2O_3	83.13	6.50 ± 2.15	+26.6
$_{con}PEI_{25\text{-}ox}$-γ-Fe_2O_3	124.1	6.36 ± 2.65	+33.0
$_{con}PEI_{25\text{-}pp}$-CAN-γ-Fe_2O_3	162.5	6.43 ± 1.60	+33.1
$_{con}$Al/PEI_{25}-CAN-γ-Fe_2O_3	70.0	7.44 ± 1.30	+35.0
$_{con}$Hy/PEI_{25}-CAN-γ-Fe_2O_3	96.3	7.37 ± 1.35	+38.6
$_{con}$Al/$PEI_{25\text{-}ox}$-CAN-γ-Fe_2O_3	118.1	6.46 ± 1.30	+53.5
$_{con}PEI_{25}$-CAN-γ-Fe_2O_3 (DoE)	85.9	6.86 ± 1.55	+20.2

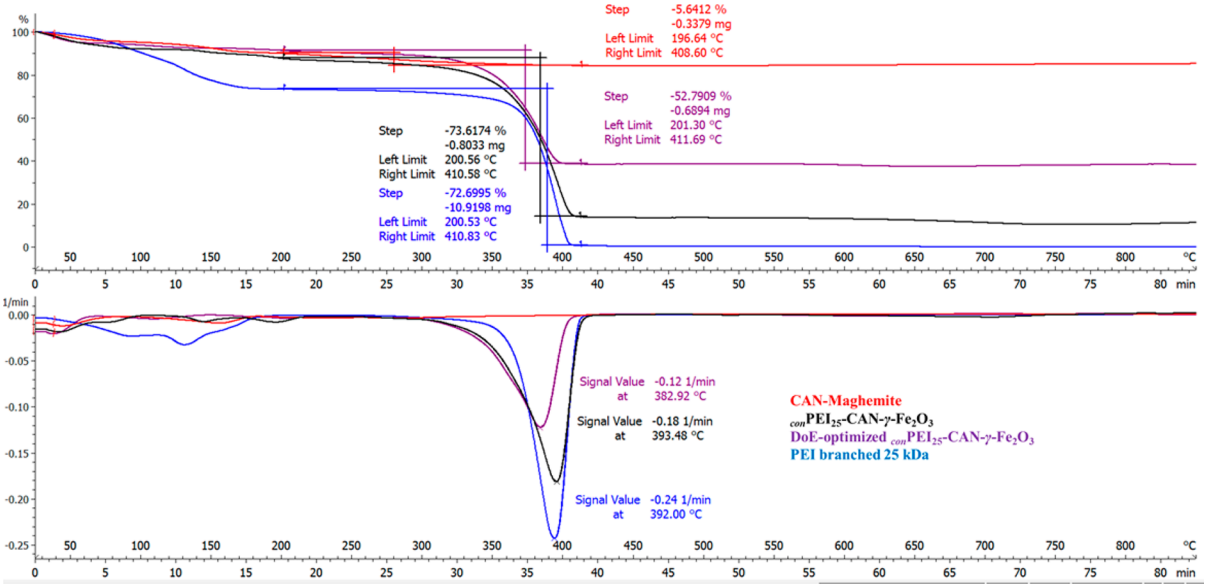

Figure 1. TGA thermogram (top) and weight loss derivative function (bottom) graphs of CAN maghemite (CAN-γ-Fe_2O_3 NPs, red curve), $_{con}PEI_{25}$-CAN-γ-Fe_2O_3 NPs (black curve; PEI ratio, 5.25), DoE-optimized $_{con}PEI_{25}$-CAN-γ-Fe_2O_3 NPs (purple curve; PEI ratio, 6.7), and PEI branched 25 kDa (blue curve). PEI weight loss calculated in a temperature range of 240−410 °C.

In order to get the best initial evaluation of which modified NPs might have the most effective potential in gene delivery, together with a reduced acute toxicity, all these modified functional nanocarriers have been systematically iv injected to mice. When compared to the starting unmodified PEI-grafted NPs, all of these optimized and chemically modified nanosystems demonstrated a clear decrease in acute *in vivo* toxicity, while maintaining their high-level *in vitro* gene delivery capabilities. Such a phase combination feature shows great promise as novel gene delivery nanosystems, which may encourage deeper studies in the near future.

2. RESULTS AND DISCUSSION

2.1. Functional PEI-Decorated Nanoparticles: NP Functionalization by a Polycationic PEI Polymer. Based upon the unique surface chemistry developed at the level of former CAN-γ-Fe_2O_3 NPs, the enabling endosomolytic-escape polycationic 25 kDa polyethylenimine polymer (*b*-PEI_{25}) was grafted onto the surface of the DoE-optimized CAN-γ-Fe_2O_3 NPs. Such a nanofabrication method afforded polycationic composite nanoparticles that disclosed a high effectiveness for an RNA electrostatic capture and an RNA-mediated gene delivery/silencing.[56,57]

Due to the multiphase composition of the surface of the PEI-decorated NPs, in order to confirm the process reproducibility and robustness and also for calibration purposes, *b*-PEI_{25}-CAN_{DOE}-γ-Fe_2O_3 NPs were fabricated again for a deeper investigation of the overall characteristics, surface functionality status, and the related quantifications. TGA, magnetic properties (SQUID), primary amine quantified amounts (Kaiser test), size distribution by TEM, hydrodynamic diameters, ζ potential, siRNA adsorption, and luciferase silencing, were among the features tested.

In the *coordination/contact two-step* method, branched 25 KDa PEI (PEI/Fe weight ratio, 5.25) polymers acting as a poly-Lewis-base species (poly$\underline{N}H_2$/poly$\underline{N}$H/poly$\underline{N}$) were reacted with CAN-γ-Fe_2O_3[57] NPs (ζ potential, +40−+50 mV; DLS, 50 nm; ddH_2O; RT; overnight; coordinative complexation/L_n ligand exchange, involving surface doping [$Ce^{3+/4+}L_n$] complexes), to afford corresponding highly hydrophilic non-aggregated 6.50 ± 2.15 nm sized (Supporting Information Figure S1; DLS hydrodynamic diameter, 83.13 nm; PDI, 0.227) and positively charged $_{con}PEI_{25}$-CAN-γ-Fe_2O_3 NPs (PEI/Fe weight ratio, 5.25). The $_{con}PEI_{25}$-CAN-γ-Fe_2O_3 NPs disclosed highly positive ζ potential values, i.e., +26.6 mV on average (Table 1).

The drop of ζ potential, in relation to the starting maghemite, is probably due to the leaving nitrate ligands that remain in the system, as counterions for the quaternary ammonium salt that was produced during the PEI primary amine complexetion by the Ce cation. An elemental ICP-AES analysis of the particles afforded elemental Ce values of 0.003615 (weight ratio Ce/Fe, 0.09538). In a surface-sensitive XPS analysis (Supporting Information Figure S2), peaks

DOI: 10.1021/acsami.5b02743
ACS Appl. Mater. Interfaces 2015, 7, 15240−15255

Table 2. Summary of the *in Vivo* Results Following the iv Injection of the Mice with Different Modified NPs[a]

NP type	siRNA dose (mg/kg)	Fe/siRNA w/w ratio	toxicity	survival rate (%)
$_{con}PEI_{25}$-γ-Fe_2O_3	1	0.315	yes (death occurred within 2 h)	0
	0.5		no	100
	0.25		no	100
$_{con}PEI_{25\text{-}ox}$-γ-Fe_2O_3	2	0.315	no	100
	1		no	100
$_{con}PEI_{25\text{-}pp}$-CAN-γ-Fe_2O_3	1	0.315	no	100
$_{con}$Al/PEI_{25}-CAN-γ-Fe_2O_3	1	0.315	no	100
$_{con}$Hy/PEI_{25}-CAN-γ-Fe_2O_3	1	0.315	no	100
$_{con}$Al/$PEI_{25\text{-}OX}$-CAN-γ-Fe_2O_3	1	0.63	no	100
$_{con}PEI_{25}$-CAN-γ-Fe_2O_3 (DoE)	1	0.157	no	100

[a]When a mouse death occurred, the survival length is indicated in the toxicity column in brackets. When no toxicity was observed, no mice death occurred at all.

characterizing the presence of $[Ce^{3+/4+}L_n]$ complexes (Ce $3d_{5/2}$ peaks; BE, 892.23 and 889.075 eV) and of the 25 KDa PEI phase (N 1s peaks for amine species; BE, 398.0−402.0 and 399.0−403.0 eV) were detected. Quite interestingly, these nanoparticles also showed characteristic peaks ascribed to the presence of nitrate anions (N 1s peaks; BE, 406.0−407.0 and 407.29 eV), most likely involved as coordinating species of the NP surface $[Ce^{3+/4+}L_n]$ complexes.

The effectiveness of the coordinative chemistry based on NP surface-localized $[Ce^{3+/4+}L_n]$ complexes has also been previously demonstrated by a saturation experiment.[52,57]

In addition, TGA data revealed a PEI amount of 73% (200−410 °C, Figure 1) and sensitive UV spectroscopy Kaiser tests[67] enabled the quantification of primary NH_2 functional groups (which might be quite useful for second step NP derivatizations or grafting) and for $_{con}PEI_{25}$-CAN-γ-Fe_2O_3 NPs afforded a value of 0.847 mmol accessible PEI NH_2 groups/(g of NPs).

Supporting Information Figures S2 and S3 reported SQUID magnetization profiles and blocking temperature (ZFC and FC graphs) for $_{con}PEI_{25}$-CAN-γ-Fe_2O_3 NPs (PEI ratio, 5.25). Clearly, and similarly to the former CAN-γ-Fe_2O_3 NPs, functional PEI-decorated NPs were found to be superparamagnetic (a hysteresis absence). They afforded an M_s value of 32.2 emu/g as well as a blocking temperature of 109−110 °C. MRI relaxivity parameter measurements were also performed.[56] These $_{con}PEI_{25}$-CAN-γ-Fe_2O_3 NPs showed excellent r_1 and r_{2*} MRI relaxivity parameters (0.103 and 168 $mmol^{-1}$ s^{-1}, respectively) toward the T_{2*} active maghemite-based NPs as contrast agents. Additional characterization data are shown in Supporting Information Figures S4−S6.

In order to assay if $_{con}PEI_{25}$-γ-Fe_2O_3 NPs can efficiently bind siRNA, we used the gel retardation assay based on the principle that small molecules will move faster through the gel than larger ones under an electric field. Various NP concentrations were incubated with a constant amount of siRNA, and then, NPs/siRNA complexes were loaded into an agarose gel and electrophoresed at 100 mA for 30 min. As we can see in Supporting Information Figure S7A, a very efficient adsorption can be obtained with a low Fe/siRNA w/w ratio of 0.063, since no free siRNA remained when compared to the control sample.

Next, to determine whether $_{con}PEI_{25}$-γ-Fe_2O_3 NPs can efficiently silence genes, we used an efficient and reliable two-gene reporter system, which is based on luciferase proteins, the 61 kDa *Firefly* and the 36 kDa *Renilla*, as stably expressed in human U2OS cells. This *Firefly* model allowed the measuring of the specific silencing, while the *Renilla* was used as a control for cell viability. *Firefly* luciferase silencing was conducted using a constant amount of siRNA (100 nM which is equal to ∼0.166 μg of siRNA) mixed with $_{con}PEI_{25}$-γ-Fe_2O_3 NPs, using different Fe/siRNA w/w ratios (0.063−0.63) (Supporting Information Figure S7B). A significant silencing of 93 ± 1% can be obtained by using an Fe/siRNA w/w ratio of 0.315, with no toxicity, since no significant change of *Renilla* activity levels occurred; however, higher ratios resulted in significant toxicity from 23 ± 3% to 37 ± 3% (0.4725 and 0.63, respectively).

Despite the fact that no efficient silencing was obtained with lower Fe/siRNA w/w ratios, and although siRNA binding was observed (Supporting Information Figure S7A), it suggests that the limiting factor for reaching high silencing capacities is the Fe/siRNA w/w ratio rather than the adsorption ability to bind the siRNA. As much as the Fe/siRNA w/w ratio increases, the amount of PEI also increases, leading to a much stronger "proton sponge" effect, that results in higher silencing capacities.

Following an intravenous injection, PEI can cause severe acute damage, leading to a rapid animal death within hours. This toxicity is due to PEI being a very positively charged polymer and, thus, being able to interact with the negatively charged membranes of red blood cells (RBCs). This interaction causes RBC aggregation and lysis, leading to thrombosis, and, finally, to animal death. Therefore, in order to determine if these nonmodified $_{con}PEI_{25}$-γ-Fe_2O_3 NPs can be injected *in vivo* into mice, without causing acute toxicity, we intravenously (iv) injected the mice with different doses of siRNA (0.25, 0.5, and 1 mg/kg), complexed with such NPs, using a Fe/siRNA w/w ratio of 0.315, which was the lower ratio that yielded efficient silencing, with no *in vitro* toxicity. Not surprisingly, the mice injected with 1 mg/kg were found dead after a period of 2 h post NP injection when compared to the mice injected with lower doses (0.5 and 0.25 mg/kg), and which were still alive (Table 2).

2.2. NP Functionalization via Selected Chemical Modifications of the NP Organic Shell. In order to provide a much higher surface chemical versatility to an NP design, the innovative $Ce^{3+/4+}$-complex coordinative chemistry might be further exploited for 25 kDa PEI toxicity mitigation, i.e., by using selective main group chemical modifications such as controlled oxidation of primary amine groups. Since PEI primary, secondary, and tertiary amines might be readily converted to corresponding neutral and/or amphoteric *hydroxylamines* (-NH−OH)/*nitroso species* (-N═O)/*nitro species* ($-NO_2$), *secondary hydroxylamines* (RR′-N−OH), and *tertiary N-oxide* $[R_3N(+)-O(-)]$, respectively, including the use of PEI hybrid mixtures with polyanionic polymers, such as

DOI: 10.1021/acsami.5b02743
ACS Appl. Mater. Interfaces 2015, 7, 15240−15255

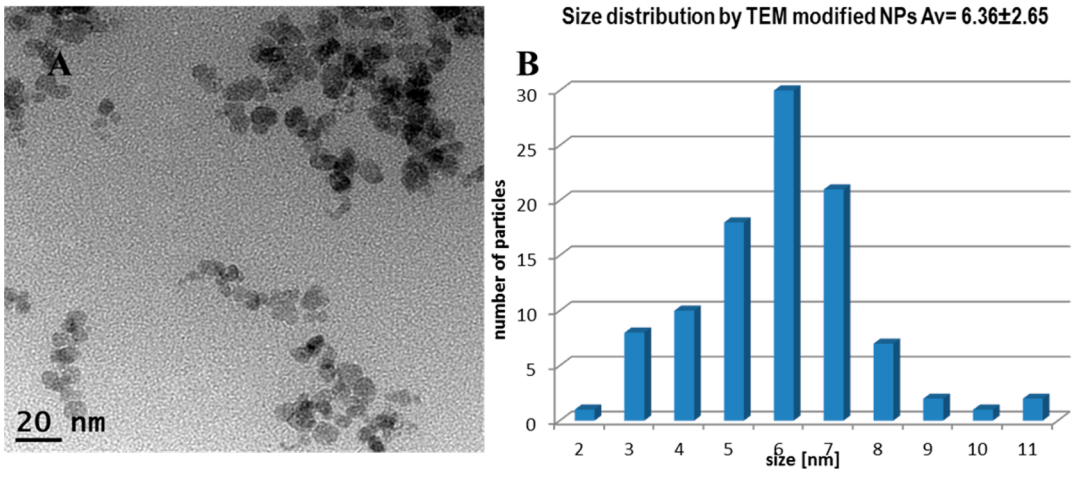

Figure 2. TEM microphotograph (A) size distribution (B) of 6.36 ± 2.65-sized PEI oxidized $_{con}PEI_{25\text{-}ox}$-CAN-γ-Fe_2O_3 NPs.

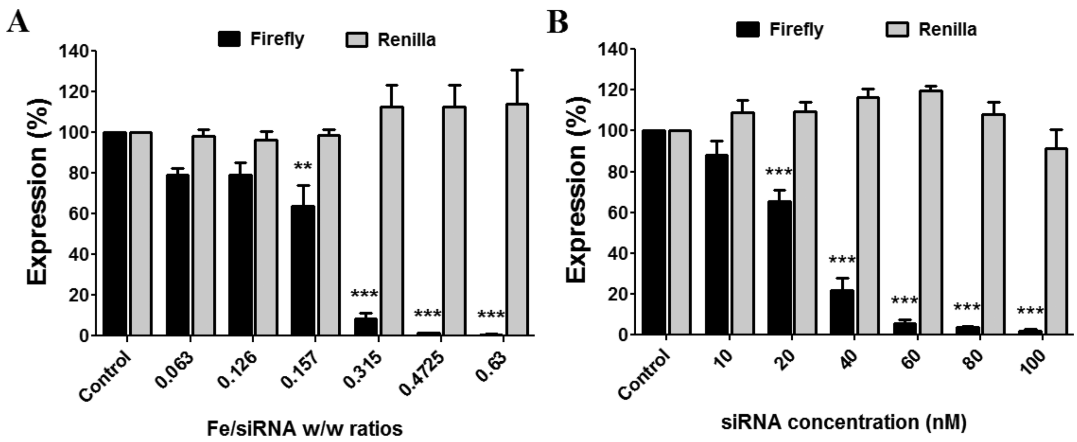

Figure 3. Luciferase silencing with $_{con}PEI_{25\text{-}ox}$-γ-Fe_2O_3 NPs with different Fe/siRNA w/w ratios and siRNA concentrations. U2OS-Luc cells (1×10^4 cells/well) were transfected with (A) *Firefly* luciferase siRNA (0.166 μg; 100 nM) and mixed with $_{con}PEI_{25\text{-}ox}$-γ-Fe_2O_3 NPs at different Fe/siRNA w/w ratios or (B) different *Firefly* luciferase siRNA concentrations were mixed with $_{con}PEI_{25\text{-}ox}$-γ-Fe_2O_3 NPs at 0.315 Fe/siRNA w/w ratios or without NPs (control). Forty-8 h later, the cells were assayed for both *Firefly* and *Renilla* luciferase activities, using the Dual-GLO Luciferase Assay System. The silencing efficacy is denoted by the luciferase activity that was normalized to the control luciferase activity. Data are expressed as mean ± SEM of three different experiments, according to the results of a two way ANOVA with a multiple comparison of a Bonferroni post hoc analysis (two asterisks (**) indicate $p < 0.01$ and three asterisks (***) indicate $p < 0.001$ vs control *Firefly*).

alginic and hyaluronic acids (Al and Hy), for an NP toxicity reduction. Such modifications can be performed in two different ways (Scheme 1)—when the PEI component is already bound on the NPs surface using a direct modification reaction performed on $_{con}PEI_{25}$-CAN-γ-Fe_2O_3 NPs (method A) and before the *b*-PEI_{25} reaction with CAN-maghemite nanoparticles (method B).

Interestingly, structural confirmation of the obtainement of some selected suggested N-oxidation moieties formed during primary amine controlled oxidation reaction, as mentioned previously, was executed in the following manner: Three separate oxidation reactions of the sole *b*-PEI_{25} phase, which possesses a measured Kaiser value of 2.3 mmol accessible PEI NH_2 groups/g (10 mg/mL solution, 20.0 mg, and 0.0008 mmol/reaction), were conducted at increasing aqueous H_2O_2 levels and were analyzed by FTIR spectroscopy. Since the controlled H_2O_2-mediated oxidation of the intermediate $_{con}$-PEI_{25}-CAN-γ-Fe_2O_3 nanoparticles has been done at a very low level (0.1% M H_2O_2), the PEI_{25} oxidation reactions (overnight, 10 °C, 250 rpm, and shaker incubator) were set up with oxidation levels of 0.1% (18.4 μL of 0.0075% solution, 0.046 μmol), 1.0% (184.3 μL of 0.0075% solution, 0.46 μmol), and 5.0% (921.5 μL of 0.0075% solution, 0.0023 mmol). Then, the resulting oxidized PEI_{25} products were lyophilized and analyzed for functionality by FTIR spectroscopy. Supporting Information Figure S8 shows all significant FTIR spectra of starting PEI_{25} (red), 0.1% oxidized PEI_{25} (blue), 1.0% oxidized PEI_{25} (teal), and 5.0% oxidized PEI_{25} (black). All three oxidized PEI_{25} phase FTIR spectra clearly disclose significant absorption peak changes relating to the formation of the N-relating oxidized species in the 1313.88−1686.81 cm^{-1} frequency range. For example, specific strong peaks appear at 1660.69 (5.0%), 1686.31 (1.0%), and 1686.81 cm^{-1} (0.1%) that are characteristic of C═N oxime bond (C═N−OH) stretchings, while such peaks are absent in the spectrum of the nonoxidized PEI_{25}. In addition, newly formed alkane nitro groups (-NO_2) can be clearly identified that exhibit both characteristic asymmetric (1476.78 cm^{-1} (0.1%)/1473.84 cm^{-1} (1.0%)/1475.49 (5.0%) cm^{-1}) and symmetric (1315.92 cm^{-1} (0.1%)/1313.88 cm^{-1} (1.0%)/1311.97 cm^{-1} (5.0%)) stretchings. Moreover, all of the strong absorption peaks appearing at 1551.97−1594.77 cm^{-1} (0.1%)/1559.14−1594.53 cm^{-1} (1.0%)/1569.04−1594.73

DOI: 10.1021/acsami.5b02743
ACS Appl. Mater. Interfaces 2015, 7, 15240−15255

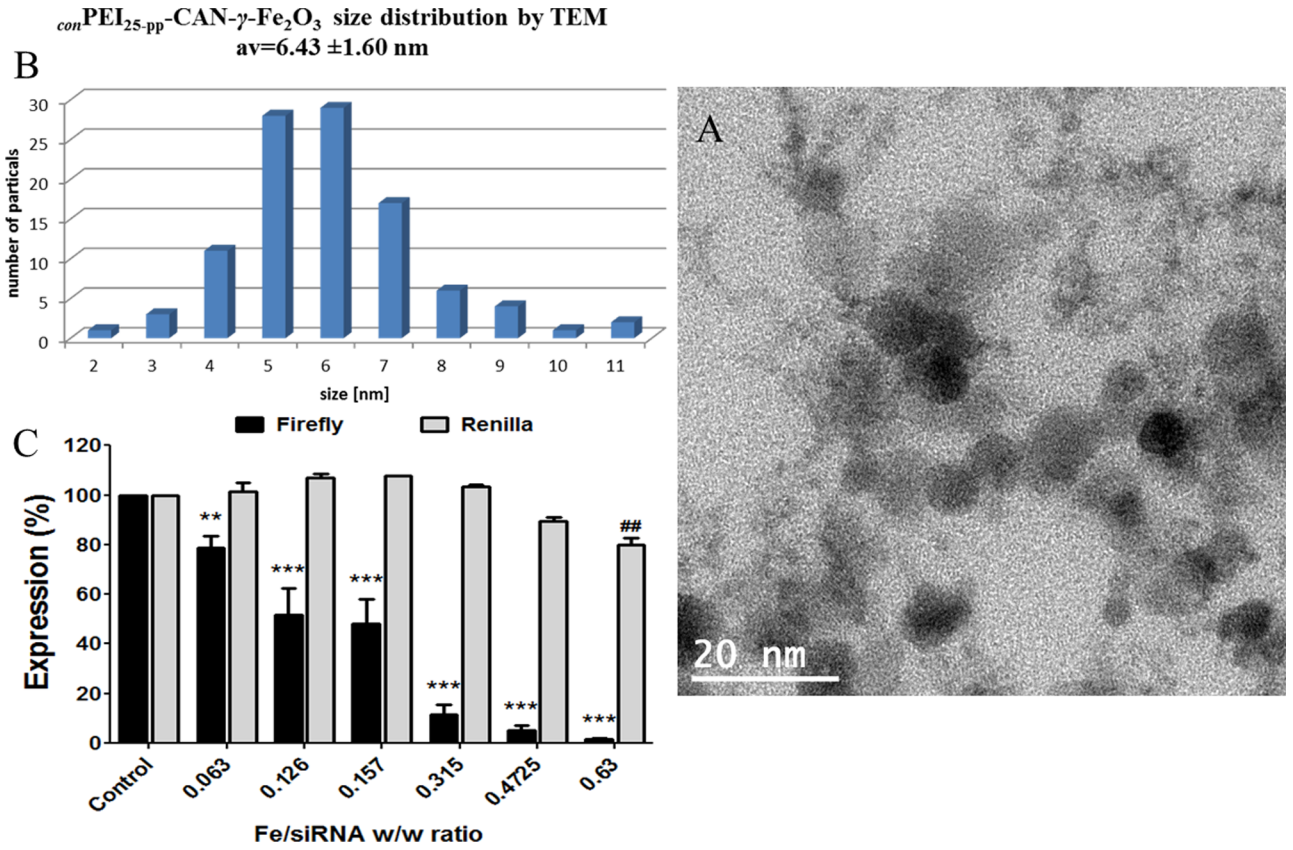

Figure 4. TEM microphotograph (A) and size distribution (B) of 6.43 ± 1.60-sized PEI oxidized $_{con}PEI_{25\text{-}pp}$-CAN-γ-Fe_2O_3 NPs and (C) NP luciferase silencing with $_{con}PEI_{25\text{-}pp}$-CAN-γ-Fe_2O_3 NPs. U2OS-Luc cells (1×10^4 cells/well) were transfected with *Firefly* luciferase siRNA (0.166 μg; 100 nM) and mixed with $_{con}PEI_{25\text{-}pp}$-CAN-γ-Fe_2O_3 NPs at different Fe/siRNA w/w ratios or without NPs (control). 48 h later, the cells were assayed for both *Firefly* and *Renilla* luciferase activities, using the Dual-GLO Luciferase Assay System. The silencing efficacy is denoted by the luciferase activity that was normalized to the control luciferase activity. Data are expressed as mean ± SEM of the three different experiments, according to the results of a two way ANOVA with a multiple comparison of a Bonferroni post hoc analysis (two asterisks (**) indicate $p < 0.01$ and three (***) indicate $p < 0.001$ vs control *Firefly*; two hatchtags (##) indicate $p < 0.01$ vs control *Renilla*).

cm^{-1} (5.0%) are also quite characteristic of N═O nitroso bond stretchings.

2.2.1. Method A: H_2O_2 Modification. In the direct reaction (method A), aqueous H_2O_2 (molar 0.1% of the primary amines as measured by the Kaiser test; 0.05−5% were also tested) was added to $_{con}PEI_{25}$-CAN-γ-Fe_2O_3 NPs, and the mixture was stirred for 24 h (orbital incubator-shaker) at 10 °C. After cleaning (centrifugal precipitation−suspension), the cleaned $_{con}PEI_{25\text{-}ox}$-CAN-γ-Fe_2O_3 NPs showed the following characteristics: average TEM (Figure 2) and DLS sizes, 6.36 ± 2.65 and124.1 nm; a positive ζ potential value, +33.0 mV (Table 1). A Kaiser test was also performed to assay the number of unmodified primary amines. A measured value of 0.800 mmol accessible PEI NH_2 groups/(g of NPs) was obtained, confirming that only a quite minimal amount of primary amines has been chemically oxidized.

These $_{con}PEI_{25\text{-}ox}$-γ-Fe_2O_3 NPs were then assayed for their ability to first silence *in vitro*. Again, in this case, a quite significant high silencing level of 91 ± 2% can be obtained with a Fe/siRNA w/w ratio of 0.315, while no toxicity was induced, even at the highest 0.63 ratio (Figure 3A). To further investigate the capacity of the NPs to silence *in vitro*, we incubated U2OS-Luc cells with different siRNA concentrations that were complexed at a constant Fe/siRNA w/w ratio of 0.315. As seen in Figure 3B, a significant reduction of 78 ± 6% and 94 ± 1% in the *Firefly* luciferase level was already obtained with a concentration of 40 and 60 nM, respectively.

To determine if the oxidation of the PEI amine groups using H_2O_2 not only results in a reduction of the *in vitro* toxicity but also in the reduction of acute *in vivo* toxicity, we iv injected mice with 1 and 2 mg/kg of siRNA complexed with NPs at a Fe/siRNA w/w ratio of 0.315. Despite oxidation occurring only with 0.1% of the PEI primary amines, one surprisingly observed that no mice death occurred even when mice were injected with a siRNA dose of 2 mg/kg (Table 2). To further confirm such results, a second 2 mg/kg dose was also injected 24 h after the first one, and here too, the mice survived with no apparent sign of distress.

2.2.2. Method B: $K_2S_2O_8$ Modification. As an alternative NP decoration process, the controlled oxidation reaction was also performed on the PEI component prior to its attachment on to the CAN-maghemite NPs' surface. First, the quantification of accessible NH_2 groups of the sole *b*-PEI_{25} was performed using the same procedure as that used for $_{con}PEI_{25}$-CAN-γ-Fe_2O_3 (Kaiser test) that led to a 2.3 mmol/g value. Then 5% of the primary amines (0.1%−5% values were tested) of *b*-PEI_{25} was reacted with potassium persulfate as the oxidizing agent ($K_2S_2O_8$, PP, 1 equiv to 5% primary amines, dissolved in 1.0 mg/mL H_2O). In a next step, the chemically modified PEI phase was reacted with CAN-maghemite NPs according to the same procedure used for the fabrication of $_{con}PEI_{25}$-CAN-γ-

DOI: 10.1021/acsami.5b02743
ACS Appl. Mater. Interfaces 2015, 7, 15240−15255

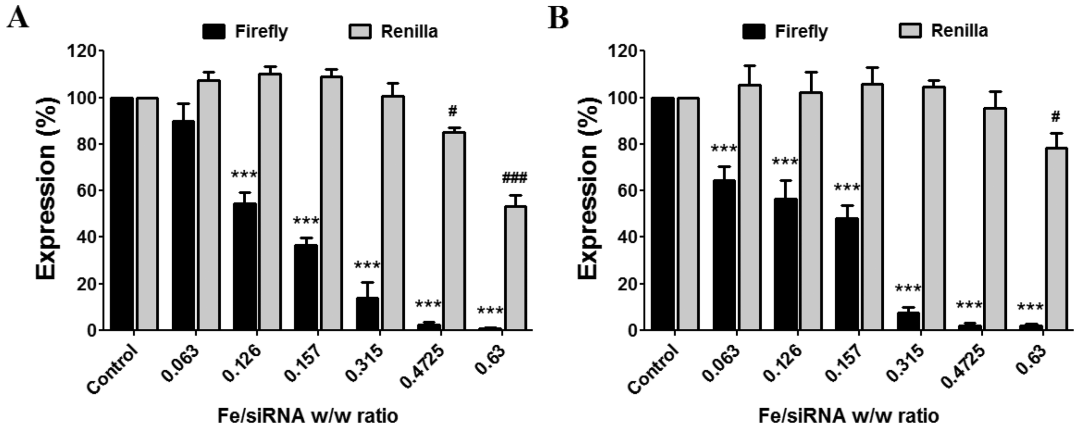

Figure 5. Luciferase silencing with CAN-γ-Fe_2O_3 functionalized with hybrid mixtures of PEI and alginic or hyaluronic acids. U2OS-Luc cells (1×10^4 cells/well) were transfected with *Firefly* luciferase siRNA (0.166 μg; 100 nM) and mixed with (A) $_{con}$Al/PEI_{25}-CAN-γ-Fe_2O_3 and (B) $_{con}$Hy/PEI_{25}-CAN-γ-Fe_2O_3 NPs at different Fe/siRNA w/w ratios or without NPs (control). 48 h later, the cells were assayed for both *Firefly* and *Renilla* luciferase activities, using the Dual-GLO Luciferase Assay System. The silencing efficacy is denoted by the luciferase activity that was normalized to the control luciferase activity. Data are expressed as mean ± SEM of the three different experiments, according to the results of a two way ANOVA with a multiple comparison of a Bonferroni post hoc analysis (three asterisks (***) indicate $p < 0.001$ vs control *Firefly* and one hatchtag (#) indicates $p < 0.05$ and three hatchtags (###) indicate $p < 0.001$ vs control *Renilla*).

Fe_2O_3. Resulting $_{con}PEI_{25\text{-}pp}$-CAN-γ-Fe_2O_3 NPs disclosed a DLS size of 162.5 nm, a positive ζ potential of +33.1 mV (Table 1), and a TEM (Figure 4) size distribution of 6.43 ± 1.60 nm.

A significant reduction of 88 ± 4% in the *Firefly* luciferase level can be obtained with a Fe/siRNA w/w ratio of 0.315 with no toxicity; however, the highest ratio of 0.63 resulted in a minor toxicity of 19 ± 2% (Figure 4).

Following the iv injection of a siRNA dose of 1 mg/kg, complexed with these NPs, and using a Fe/siRNA w/w ratio of 0.315, no mice death was observed post the injections (Table 2).

Unexpectedly, and although showing no acute *in vivo* toxicity, both $_{con}PEI_{25\text{-}pp}$-CAN-γ-Fe_2O_3 and $_{con}PEI_{25\text{-}ox}$-CAN-γ-Fe_2O_3 NPs disclosed a slightly more positive ζ potential value when compared to that of $_{con}PEI_{25}$-CAN-γ-Fe_2O_3 NPs (+33 mV vs +26.6 mV). This last piece of data is likely indicative of NP surface-localized $PEI_{25\text{-}ox}$ polymer rearrangements, mediated by doping $[CeL_n]^{3+/4+}$ metal cations/complexes. The PEI_{25} oxygenated oxidized amine species mentioned earlier have a thermodynamically stronger O-relating Lewis base character (hardness) than nonoxidized related amine groups. This enables more effective O (PEI_{25ox})- vs N (PEI_{25})-based competitive coordinative covalent interactions within the NP surface cationic $[CeL_n]^{3+/4+}$ complexes.[62,63,68]

When a hydroxylamine group coordinates with the $Ce^{3+/4+}$cation/complex, two possibilities exist. First, a nitro ligand is in the leaving group, but since a proton is released from the hydroxylamine species, an HNO_3 molecule is thus formed and eliminated during centrifugal washing and cleaning steps. The second option is an internal $Ce^{3+/4+}$ cation/complex coordinated PEI amine function in which case the hydroxylamine leaving proton causes protonation of this leaving amine ligand/function with an outer presentation, which may explain such incremental ζ potential values. These two optional cases might readily explain the toxicity reduction of the corresponding NPs. When nitrate ligands are leaving ligands, the reduction is caused by a smaller number of primary amines, oxidized to hydroxylamines, which are now coordinatively bounded onto $Ce^{3+/4+}$ cations. In the second case, amine leaving groups are already protonated, so they cannot trap any additional proton from the outside contacting biological system. In both cases, since the oxygen−$Ce^{3+/4+}$ cation bond is thermodynamically stronger than the N−Ce bond, any leaching of PEI from the surface to the biological system is also reduced, and therefore, the toxicity is also decreased. This form of toxicity control is quite innovative. Previous studies[66] used H_2O_2 in order to oxidize amine groups present on PEI/DNA complexes without the use of any nanoscale carrier. This resulted in a decreased charge, which led to PEI toxicity mitigation. However, in the case of modified $_{con}PEI_{25}$-CAN-γ-Fe_2O_3 NPs, the component charge was increased suggesting that the mechanism of toxicity mitigation was acting in a different way.

2.2.3. Method A: LbL Modifications. Other modified systems included polycationic coordinated PEI nanocarriers that were surface engineered using a reaction with the fully biocompatible polyanionic (polyCOOH) polysaccharides such as alginic (Al; MW, 120−190 kDa) and hyaluronic (Hy; MW, 15−30 kDa) acid, of various molecular weights, onto the same polyaminated nanocarriers; this was in order to afford novel "stealth" surface-modified nanocarriers that were tested for silencing capabilities and for toxicity/nontoxicity profiling. Various w/w Fe/alginate ratios were tested for this contact noncovalent layer-by-layer (LbL) electrostatic attachment. According to the hydrodynamic diameter (measured by DLS) and the TEM size distribution (Supporting Information Figure S9) of the resulting nanocarriers (NCs), *highly stable* and monodisperse $_{con}PEI_{25}$-Al-CAN-γ-Fe_2O_3 NPs were obtained in 70.0−84.7 (DLS) and 7.44 nm (TEM), respectively; average size ranges with ζ potential values were observed in a +35.0 to +37.0 mV value range (Table 1).

Furthermore, the conjugation between the alginic acid phase and the $_{con}PEI_{25}$-CAN-γ-Fe_2O_3 NPs was confirmed by FTIR spectroscopy (Supporting Information Figure S10). Characteristic peaks of pristine alginic acid (COOH; blue line) and $_{con}PEI_{25}$-Al-CAN-γ-Fe_2O_3 NPs (red line) appeared at 1626.9 cm^{-1}. The adsorption peaks that appeared at 1566.05 and 1475.48 cm^{-1} of the $_{con}PEI_{25}$-Al-CAN-γ-Fe_2O_3 (red line) might be attributed to the stretching modes of the N−H bonds related to the PEI phase. O−H stretching vibration modes

DOI: 10.1021/acsami.5b02743
ACS Appl. Mater. Interfaces 2015, 7, 15240−15255

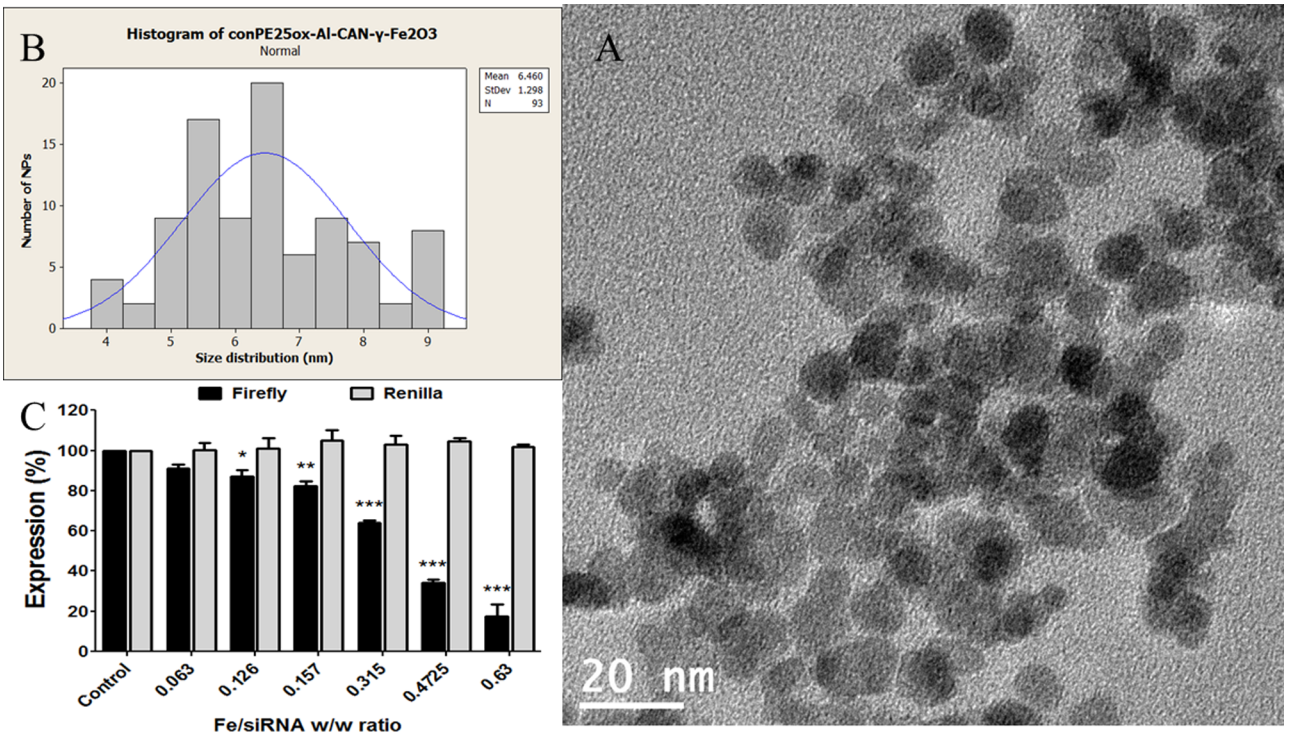

Figure 6. (A) TEM photograph, (B) size distribution histogram of averaged 6.46 nm sized $_{con}$Al/PEI$_{25\text{-}ox}$-CAN-γ-Fe_2O_3 NPs, and (C) *Firefly* luciferase gene silencing results in U2OS-Luc cells with luciferase silencing with $_{con}$Al/PEI$_{25\text{-}ox}$-CAN-γ-Fe_2O_3 NPs. U2OS-Luc cells (1×10^4 cells/well) were transfected with a *Firefly* luciferase siRNA (0.166 μg; 100 nM) and mixed with $_{con}$Al/PEI$_{25\text{-}ox}$-CAN-γ-Fe_2O_3 NPs at different Fe/siRNA w/w ratios or without NPs (control). 48 h later, the cells were assayed for both *Firefly* and *Renilla* luciferase activities, using the Dual-GLO Luciferase Assay System. The silencing efficacy is denoted by the luciferase activity that was normalized to the control luciferase activity. Data are expressed as mean ± SEM of the three different experiments, according to the results of a two way ANOVA with a multiple comparison of a Bonferroni post hoc analysis (one asterisk (*) indicates $p < 0.05$, two asterisks (**) indicate $p < 0.01$, and three asterisks (***) indicate $p < 0.001$ vs control *Firefly*).

appeared at 3421.98 and 3138.02 cm^{-1} in both spectra. The peaks appearing at 2934.1 and 2848.73 cm^{-1} were attributed to the C−H stretching modes of the PEI (red line). Moreover, the C−O stretching vibrations for secondary alcohols appeared at 1121.18 cm^{-1} in both spectra. The peaks observed at 575.84 and 400 cm^{-1} (red line) are part of the fingertip adsorption region of starting CAN-γ-Fe_2O_3 NPs.

Next, we examined the same chemical derivatization method of $_{con}$PEI$_{25}$-CAN-γ-Fe_2O_3 core NPs for a *noncovalent* nanocarrier surface modification, using a similar polyanionic biocompatible and biodegradable Hy phase. Similarly, various w/w Fe/hyaluronate ratios were tested for a contact electrostatic attachment/surface modification of the nanocarrier surface. Hydrodynamic diameters and size distributions of the resulting highly stable (aqueous media) and monodisperse $_{con}$PEI$_{25}$-Hy-CAN-γ-Fe_2O_3 NPs were obtained by DLS and TEM, i.e., 92.96−187.10 and 7.37 nm, respectively (Supporting Information Figure S11), while the ζ potential values were found positive in a +34.0 to +45.0 mV range (Table 1).

Again, FTIR spectroscopy confirmed the conjugation/adsorption/interaction between both hyaluronic acid and the PEI/CAN maghemite NP components (Supporting Information Figure S12, hyaluronic acid (blue line) and $_{con}$PEI$_{25}$-Hy-CAN-γ-Fe_2O_3 (red line)). Amide characteristic peaks at 1633 cm^{-1} are seen in both spectra. Additionally, NH stretchings of *b*-PEI$_{25}$ molecules appear at 1475.48 cm^{-1} (red line). The peaks appearing at 1049.84 (red line) and 1046.03 cm^{-1} (blue line) could be attributed to C−O−C stretchings of hyaluronic acid in both spectra. The peaks detected at 575.84 and 400 cm^{-1} (red line) are part of the fingertip region of starting CAN-γ-Fe_2O_3 NPs.

Although both $_{con}$Al/PEI$_{25}$-CAN-γ-Fe_2O_3 and $_{con}$Hy/PEI$_{25}$-CAN-γ-Fe_2O_3 NPs were fabricated in an effort to produce LbL nanosystems, their characteristics (especially positive ζ potential measurements) imply that such an LbL NPs surface engineering lacked effectiveness, probably due to the unique coordinating $[CeL_n]^{3+/4+}$ cations present on the NPs surface.

Both $_{con}$Al/PEI$_{25}$-CAN-γ-Fe_2O_3 and $_{con}$Hy/PEI$_{25}$-CAN-γ-Fe_2O_3 NPs were thus also tested for their ability to silence the luciferase gene (dual luciferase system). Both types of NCs retained their capacities to efficiently silence the luciferase gene with a low Fe/siRNA mass ratio (0.315) (Figure 5), as we had previously obtained for former $_{con}$PEI$_{25}$-CAN-γ-Fe_2O_3 NPs (83 ± 6% for $_{con}$Al/PEI$_{25}$-CAN-γ-Fe_2O_3 NPs and 92 ± 2% for $_{con}$Hy/PEI$_{25}$-CAN-γ-Fe_2O_3 NPs).

Next, both engineered NPs were injected into the mice to evaluate their acute *in vivo* toxicity by iv injection of 1.0 mg/kg of siRNA, complexed with NPs, at the best Fe/siRNA w/w ratio of 0.315. Also in this case, all of the injected mice survived following both NP injections (Table 2).

Despite this addition of polyanionic polymers that did not reduce NC surface charges, when compared to the original $_{con}$PEI$_{25}$-CAN-γ-Fe_2O_3 NPs (ζ potential, +35.0 mV; Table 1), all iv injections did not result in any animal death. The partial replacement of PEI by hyaluronic or alginic acids resulted in a functionalized NP surface where the PEI chains are more externally accessible than NPs surface coordinated polyanionic polymers. Thus, due to ζ potential measurements reflecting only the charge of the extreme outer shell of NPs, we noticed

DOI: 10.1021/acsami.5b02743
ACS Appl. Mater. Interfaces 2015, 7, 15240−15255

almost no change in terms of charges between both types of NPs.

2.2.4. Method A – Combined H_2O_2 and LbL Modification. As previously demonstrated, one may significantly reduce the intrinsic toxicity of PEI-made polycationic shell compositions, by chemically transforming the PEI amine functions into corresponding N-oxidized species by using a mild oxidative liquid process. The amphoteric poly-*N*-oxide character of the oxidized PEI shell, obtained in such a manner, preserved quite a high 95% *Firefly* luciferase gene silencing capability at a low 0.315 Fe/siRNA weight ratio. Therefore, this innovative oxidative process was applied to a wider range of polycationic CAN-γ-Fe_2O_3 NP-based delivery systems, i.e., exploring the effectiveness of the H_2O_2-mediated oxidative process for the combinatorial engineering of $_{con}PEI_{25\text{--}ox}$-Al-CAN-$\gamma$-$Fe_2O_3$ mixed with NP shells toward both an effective and safe NP siRNA electrostatic capture and an *in vitro*/*in vivo* delivery. The toxicity mitigation results (Figure 6) for $_{con}PEI_{25\text{--}ox}$-Al-CAN-$\gamma$-$Fe_2O_3$ NPs showed a significant reduction of the NP polycationic character. The hydrodynamic diameter and ζ potential of the resulting *highly stable* (aqueous media) and monodisperse $_{con}PEI_{25\text{--}ox}$-Al-CAN-$\gamma$-$Fe_2O_3$ NPs were obtained in a 102.5−104.8 nm scale range and positive ζ potential values in a +48.9 to +53.5 mV range (Table 1).

Compared to previous modifications, we noticed that these NPs are much less potent in terms of silencing, since a reduction of 82 ± 5% in the *Firefly* levels can be observed with only the highest Fe/siRNA w/w ratio of 0.63 (Figure 6).

However, the mice that were iv injected with 1.0 mg siRNA/kg, complexed onto the corresponding NPs using a Fe/siRNA w/w ratio of 0.63, survived, despite the high amount of injected NCs when compared to the previous ones (Table 2).

2.3. Process Optimization by DoE. In addition to the described modifications, and since most of the surface modifications were performed after a *b*-PEI_{25} conjugation to a CAN-γ-Fe_2O_3 NC surface (method A), in order to improve the robustness of the process and to globally optimize it, a DoE (design of experiment) study was also performed, in order to globally optimize the basic PEI coordination process ($_{con}PEI_{25}$-CAN-γ-Fe_2O_3 NPs fabrication) upon which all of the chemical modifications mentioned earlier rely.

A DoE study allows the change of more than one factor/reaction condition at a time, even when a lot of factors are tested, and therefore, fewer experiments are needed for the optimization process. This approach also enables the study of how the factors interact with each other and how that interaction influences the final results, which is not available in a regular optimization study. The DoE study of the PEI decoration reaction aims to deliver robust reaction conditions that eventually lead to a maximal silencing at a minimal Fe/SiRNA ratio (in order to reduce the needed Fe quantities), and with a minimal amount of PEI (measured by TGA). Reaction conditions, such as the reaction temperature, can influence the dynamics of how the *b*-PEI_{25} polycationic polymer is bound onto the NP surface (for example, lowering the temperature can cause a more energy deficient steric form of binding onto the core of the NP surface).

The software MINITAB 16 DoE (version 16.2.4, Minitab Inc.) was used and three potentially influential reaction factors have been identified and set up at both low and high evolution values that afforded a partial factorial design with two repeats. This DoE design provided a corresponding series of randomly setup experiments (Table 1)—i.e., eight experiments, to which three center points were added, were executed accordingly, with the following important factors: the incubation time (4 and 48 h), the PEI amount (or PEI/Fe ratio, two values of 2 and 7), and the incubation temperature (two values, 15 and 35 °C) (Table 3). Therefore, the optimal DoE-based responses

Table 3. Experimental Array ($_{con}PEI_{25}$-CAN-γ-Fe_2O_3) and Corresponding Process Responses

PEI/Fe ratio	incubation time (h)	temp (°C)	% PEI (TGA)	% maximal silencing	Fe/SiRNA silencing ratio	NP no.
7	4	15	80.32	96	0.315	DoE-1
4.5	26	25	47.92	93	0.63	DoE-2
7	48	35	60.66	88	0.315	DoE-3
2	48	15	39.65	19	0.63	DoE-4
2	4	35	56.76	11	0.63	DoE-5
4.5	26	25	84.13	89	0.4725	DoE-6
4.5	26	25	71.93	80	0.63	DoE-7
2	48	15	74.51	85	0.4725	DoE-8
7	4	15	65.31	100	0.4725	DoE-9
7	48	35	80.85	97	0.315	DoE-10
2	4	35	60.52	80	0.63	DoE-11

investigated were as follows: both percentages of the maximal silencing, the PEI amounts (TGA measurements), and the resulting Fe/SiRNA silencing ratios (Table 3).

Full analysis of these response data was performed using the MINITAB 16 DoE software, and both most important process factors and first rank interactions were clearly identified using Pareto charts of standardized effects, 2D contour plot graphs, and full interaction plot matrices, as described in Figure 7. The Pareto chart is an example of an analysis that reveals what are the most significant factors for a certain response. The Pareto chart in Figure 7 indicates that the most significant factor influencing the Fe/SiRNA ratio that is needed for maximal silencing is the PEI/Fe ratio in the reaction since it is the only one that crosses the red line and is therefore statistically significant.

An additionally important form of analysis is the interaction plot for a chosen response. It basically provides subsequent process information if there is an interaction between the two different factors examined for that response. When the two graphs correspond, there is no interaction between the two factors. When they are significantly different, and even cross each other, it means that there is a strong interaction between the two, and a change in one of these factors will lead to a change in the other, for optimal results. These two factors are qualified as being "connected".

Another analysis is the 2D contour plot. In this analysis, in a way similar to a topographic map, two of the factors are shown in the *X* and *Y* axes, while the chosen response is color coded at the *z* axis. Figure 7 clearly shows that, for a maximal 100% silencing, a PEI/Fe ratio higher than 3.5 is required. That 100% silencing can be reached in all incubation times according to Figure 7. Nevertheless, a strong interaction exists between the incubation time and the reaction temperature, so if a change in temperature is required to attain the optimal set of conditions, a change of incubation time will be needed accordingly.

After analysis (MINITAB 16 DoE software profile optimizer module, Supporting Information Figure S13), an optimal set of conditions was calculated (PEI/Fe ratio of 6.7, 48 h incubation

DOI: 10.1021/acsami.5b02743
ACS Appl. Mater. Interfaces 2015, 7, 15240−15255

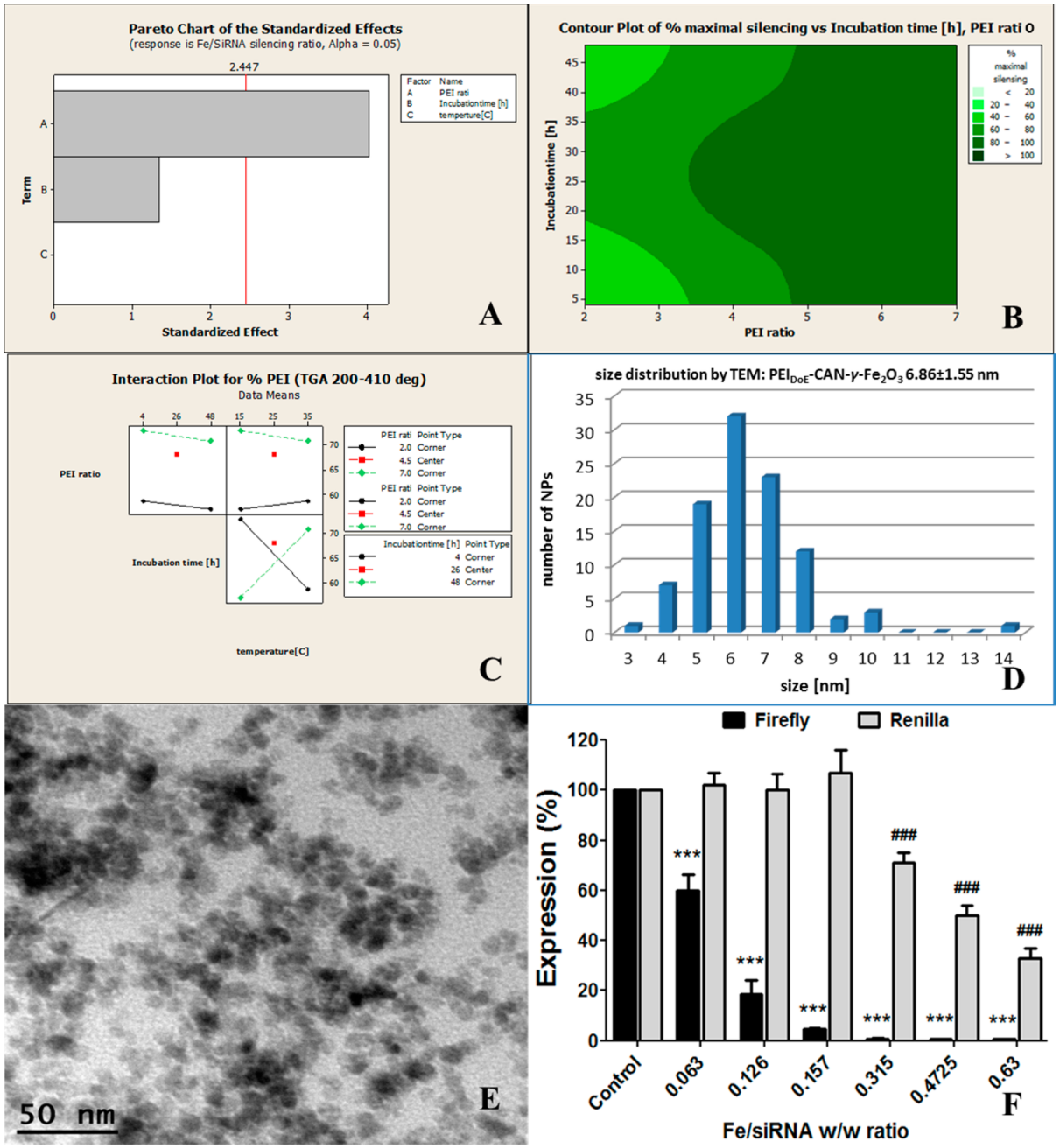

Figure 7. DoE-optimized fabrication of PEI_{DOE}CAN-maghemite NPs: (A) Pareto chart of standardized effects for the response of a Fe/SiRNA silencing ratio, (B) 2D contour plot of the percent of maximal silencing vs incubation time (h) and PEI ratio, (C) full interaction plot matrices for the percent PEI (TGA) factor, (D) size distribution by TEM (6.86 ± 1.55 nm), (E) TEM image, and (F) luciferase silencing in the U2OS-Luc cells.

time, and a reaction temperature of 15 °C) and globally optimized $_{con}PEI_{25}$-CAN-γ-Fe_2O_3 NPs were fabricated accordingly and characterized.

The following data for the resulting DoE-optimized $_{con}PEI_{25}$-CAN-γ-Fe_2O_3 NPs were obtained in a reproducible manner: (i) an average NP hydrodynamic size (DLS) of 85.9 nm, (ii) a positive ζ potential of +20.2 mV, and (iii) a weight PEI percentage of 52.8% (Table 1, Figures 1 and 7). At this stage, such functional NPs were further characterized by various combined analytical, spectroscopic, and microscopic methods. For example, a Kaiser test was performed to quantify the primary amines on the NP surface at 0.854 mmol of NH_2/(g of NPs), and the NP size distribution by TEM (100 analyzed objects, ImageJ software analysis) was also measured (6.86 ± 1.55 nm, Figure 7). A quick comparison of NPs size distributions of $_{con}PEI_{25}$-CAN-γ-Fe_2O_3 before and after the DoE study reveals a narrower Gaussian graph after the DoE was performed. Measurements of the DoE-optimized NP hydrodynamic diameter were in the range of 72.0−86.0 nm (PDI, 0.14−0.19) with a ζ potential in a +18.3−20.2 mV value range (various batches).

As we can see in Figure 7F, the DoE process indeed optimized the efficacy of the $_{con}PEI_{25}$-CAN-γ-Fe_2O_3 NPs to silence, since we can already achieve a significant silencing of 95 ± 0.5% by using quite a low Fe/siRNA w/w ratio of 0.157. However, these NPs seem to be more toxic *in vitro* when compared to the original $_{con}PEI_{25}$-CAN-γ-Fe_2O_3 NPs as the

DOI: 10.1021/acsami.5b02743
ACS Appl. Mater. Interfaces 2015, 7, 15240−15255

Renilla levels decreased from 28 ± 3% to 67 ± 4% when using Fe/siRNA w/w ratios of 0.315 to 0.63, respectively.

Despite the DoE study being mainly performed to improve the robustness of the process, these DoE-optimized $_{con}PEI_{25}$-CAN_{DoE}-γ-Fe_2O_3 NPs were also injected intravenously into mice with a siRNA dose of 1.0 mg/kg complexed with NPs at a Fe/siRNA w/w ratio of 0.157. This ratio yielded a significant and satisfying silencing in the luciferase assay. Since no chemical modifications of the PEI component were performed in these NPs, we were surprised that following the iv injection of these NPs into the mice, no animal death was observed (Table 2).

The observed mitigation of the acute *in vivo* toxicity can be readily explained by two different observations. The first, and despite the increased amount of PEI and the increased reaction time of the DoE-optimized reaction, the percentage of PEI measured by TGA (Figure 1) was ∼20% lower after the DoE optimization, while the silencing efficiency was not harmed. This also suggests that the coordinative attachment of PEI to the surface is a thermodynamically controlled process. Since the reaction temperature is decreased in the DoE-optimized case, meaning that the energy from the environment decreases, the PEI is likely coordinatively attached in a most stable and energy deficient way. Once a stronger bond is formed, it is less likely that a surface-bound PEI will leach toward the external contacting biological medium and, thus, cause toxic effects; so even though a lower quantity of PEI is found on the surface, the silencing effect is not harmed.

3. CONCLUSIONS

It was demonstrated that very innovative magnetic $Ce^{3+/4+}$ cation-doped maghemite (γ-Fe_2O_3) NPs might be successfully decorated ("contact" decoration process—*coordinative mode* of $Ce^{3+/4+}$ cation complexation of N-/O-containing organic species acting as Lewis bases) by variable weight ratios of 25 kDa branched PEI (*b*-PEI_{25}), PEI_{25}/hyaluronic acid (PEI_{25}/Hy), and PEI_{25}/alginic acid (PEI_{25}/Al). This specific nanocarrier surface engineering was designed for PEI toxicity mitigation in *in vivo* applications of corresponding therapy-loaded, tumor-targeting nanocarriers. The highly stable and monodisperse PEI_{25}/Hy and PEI_{25}/Al NCs were first obtained using this kind of methodology. In addition, both a controlled oxidation technique and a DoE study effectively decreased the original $_{con}PEI_{25}$-CAN_{DoE}-γ-Fe_2O_3 NPs acute toxicity *in vivo*. The silencing capability of such functional nanocarriers was shown to be strictly dose-dependent, i.e., increasing when using additional amounts of NPs while tested NPs surface chemical modifications did not ever compromise NPs *in vitro* silencing capabilities (acute *in vivo* toxicity mitigation). More specifically, NPs such as $_{con}Al/PEI_{25}$-CAN-γ-Fe_2O_3, $_{con}Hy/PEI_{25}$-CAN-γ-Fe_2O_3, and especially $_{con}PEI_{25\text{-}ox}$-γ-Fe_2O_3 NCs disclosed effective mitigated toxicity at even higher doses, showing a great potential as innovative siRNA delivery agents.

4. EXPERIMENTAL SECTION

4.1. PEI-Decorated CAN-Stabilized Maghemite Nanoparticles ($_{con}PEI_{25}$-CAN-γ-Fe_2O_3 NPs). The CAN-γ-Fe_2O_3 NPs[56] aqueous suspension arising from CAN-mediated high-power ultrasonication (Sonics, Vibra cell, 750 W, power modulator setup at 25%, Ti horn 30 min, 0 °C, dry inert argon atmosphere), 1 mL, (Fe: 3.88 mg/mL − 3.88 mg total Fe, 0.0696 mmol Fe, ICP measurement), was diluted to 28.0 mL using Milli-Q purified H_2O. Then, 20.136 mg of 25 kDa branched PEI (0.8 μmol; PEI/Fe weight ratio, 5.25) was added at room temperature to the NP suspension as an aqueous solution (10.0 mg of PEI/mL), and the medium was shaken overnight at room temperature (orbital shaker). At the completion of such a mild PEI contacting/NP surface decoration, the resulting crude $_{con}PEI_{25}$-CAN-γ-Fe_2O_3 NPs were washed three times (3 × 10 mL of ddH_2O) using an Amicon Ultra-15 centrifugal filter device (100 K), operated at 4000 rpm (for 12 min), followed by a size exclusion process performed using centrifugation (8000 rpm/min, 16 min, 18 °C and 7000 rpm, 10 min, 18 °C) to afford cleaned $_{con}PEI_{25}$-CAN-γ-Fe_2O_3 NPs (PEI/Fe weight ratio, 5.25).

4.2. H_2O_2-Mediated Controlled PEI Shell Oxidation of $_{con}PEI_{25}$-CAN-γ-Fe_2O_3 NPs: Optimized Fabrication of Corresponding PEI Oxidized $_{con}PEI_{25\text{-}ox}$-CAN-γ-Fe_2O_3 NPs. In a typical reaction, 3.1 mL of the former aqueous $_{con}PEI_{25}$-CAN-γ-Fe_2O_3 (with an ICP concentration of Fe = 0.41 mg/mL, Fe = 1.0664 mg, and NPs concentration ∼4.1 mg/mL aqueous suspension) was further diluted to 14 mL of (ddH_2O) in a conic plastic centrifuge tube. Then, 0.341 mL of a 0.000075 wt % aqueous solution of H_2O_2 in Milli-Q purified H_2O was added (0.1% molar of the starting NP primary amines (NH_2) as measured by a Kaiser test of 0.000847 mmol of NH_2/(mg of NPs), together with a ratio that was investigated at 0.05−5%), after which the reaction mixture was shaken at 250 rpm at 10 °C overnight (cooled shaker incubator). The resulting reaction mixture was then washed by Milli-Q purified H_2O (3 × 8 mL), using an Amicon Ultra-15 centrifugal filter t (100 K) operated at 4000 rpm (centrifuge) for 5−6 min (RT, 18 °C), and was then concentrated to 0.5−1 mL by water evaporation (ICP-AES, Fe = 0.41 mg/mL).

4.3. $K_2S_2O_8$ (Potassium Persulfate)-Mediated Controlled *b*-PEI_{25} Oxidation and the Reaction with CAN-γ-Fe_2O_3 NPs toward Corresponding PEI Oxidized $_{con}PEI_{25\text{-}pp}$-CAN-γ-Fe_2O_3 NPs. First, potassium persulfate (1 mg/mL solution in H_2O, 0.02875 mmol, 7.77 mg) was added dropwise to a solution of branched 25 kDa polyethylenimine (10 mg/mL H_2O solution, 250 mg, 0.01 mmol of *b*-PEI_{25}, and 0.575 mmol of primary amines) in order to modify 5% of the PEI primary amines. Then, 1 mL of core CAN-maghemite nanoparticles (Fe = 1.48 mg/mL, 1.48 mg Fe) was diluted with 20 mL of H_2O, and the modified PEI solution (10 mg/mL,0.777 mL, 7.77 mg, PEI/Fe in this ratio of 5.25) was added; the reaction mixture was shaken overnight at RT.

The NP product was purified by Milli-Q purified H_2O (3 × 8 mL) using a filter centrifugation (Amicon Ultra-15 centrifugal filter tube with a 100 kDa cutoff, at 4000 rpm for 10 min), followed by a size exclusion process performed using centrifugation (8000 rpm/min, 15 min, 18 °C and 7000 rpm, 5 min, 18 °C) to afford cleaned $_{con}PEI_{25\text{-}pp}$-CAN-γ-Fe_2O_3 NPs (using a PEI/Fe weight ratio of 5.25). The dispersion was then concentrated by vacuum evaporation to a final volume of 2 mL.

4.4. $_{con}Al/PEI_{25}$-CAN-γ-Fe_2O_3 NPs: Fabrication Protocol. $_{con}PEI_{25}$-CAN-γ-Fe_2O_3 NPs containing a $Ce^{3+/4+}$ cation-coordinated $_{con}PEI_{25}$ polymeric phase was mixed with the polyanionic alginic acid (Al) component aqueous solution (MW, 120−190 kDa; 5 mg/mL) at various w(Fe)/w(Al) ratios for a contact *noncovalent* LbL electrostatic mode of attachment. The w(Fe)/w(Al) ratios which were investigated are 1%, 10%, 30%, and 50% alginic acid. The optimal ratio determined by luciferase assay *in vitro* (section 4.8) was 30 wt % alginic acid: 0.22 mg/(1.83×10^{-6} mmol) alginic acid was added to 1.0 mL of $_{con}PEI_{25}$-CAN-γ-Fe_2O_3 NPs (aqueous suspension, section 4.1), and the medium was diluted with an additional 20 mL of Milli-Q purified H_2O followed by an overnight incubation (orbital shaker, 250 rpm, 20 °C). The resulting hydrophilic highly stable $_{con}Al/PEI_{25}$-CAN-γ-Fe_2O_3 NPs were then washed with Milli-Q purified H_2O (3 × 10 mL) using an Amicon Ultra-15 centrifugal filter device (100 K) operated at 4000 rpm (centrifuge) for 5 min (at room temperature), and then redispersed in H_2O (1.0 mL) for storage and/or gene silencing experiments.

Corresponding selected characterization data (NPs for an optimal 30% (w/w) component ratio regarding *in vitro* gene silencing) are mentioned in Table 1 and Supporting Information Figure S9.

4.5. $_{con}Hy/PEI_{25}$-CAN-γ-Fe_2O_3 NPs: Fabrication Protocol. The corresponding 4.4 protocol was similarly extended to the use of a

DOI: 10.1021/acsami.5b02743
ACS Appl. Mater. Interfaces 2015, 7, 15240−15255

polyanionic biodegradable biocompatible 15−30 kDa hyaluronic acid (1.0 mg/mL aqueous solution) instead of the formerly used alginic acid phase. The w(Fe)/w(Hy) ratios which were investigated are 1%, 10%, 30%, and 50% hyaluronic acid. The optimal ratio determined by luciferase assay *in vitro* (section 4.9.4) was found to be 10% hyaluronic acid: 0.023 mg/(1.57×10^{-6} mmol) of Hy acid was added respectively to 1.0 mL of NPs suspended in Milli-Q purified H_2O and incubated overnight (at room temperature). The resulting NCs were washed with water (3 × 10 mL) using an Amicon Ultra-15 centrifugal filter device (100 K) at 4000 rpm for 5 min.

Corresponding selected characterization data (NPs for an optimal 10% (w/w) component ratio regarding *in vitro* gene silencing) are mentioned in Table 1 and Supporting Information Figure S11.

4.6. Preparation of $_{con}PEI_{25\text{-}ox}$-Al-CAN-γ-Fe_2O_3 NPs. 30% (weight ratio, former optimal ratio of $_{con}$Al/PEI_{25}-CAN-γ-Fe_2O_3 NPs fabrication) alginic acid was tested for this contact electrostatic attachment. The following amount of 0.22 mg/(1.83×10^{-6} mmol) alginic acid was added to 1.0 mL of $_{con}PEI_{25\text{-}ox}$-CAN-γ-Fe_2O_3 NCs dispersed in H_2O and incubated overnight (at room temperature). The resulting NCs were washed with ddH_2O (3 × 10 mL), using an Amicon Ultra-15 centrifugal filter device (100 K) at 4000 rpm for 5 min. The conjugation between the alginic acid phase and $_{con}PEI_{25}$-ox-CAN-γ-Fe_2O_3 NPs was confirmed by DLS, ζ potential, and FTIR. These characterization data can be found in Table 1 and Figure 6.

4.7. $_{con}PEI_{25}$-CAN-γ-Fe_2O_3: DoE Global Optimization of the Nanofabrication Process of PEI-Functionalized NPs. The former corresponding CAN-γ-Fe_2O_3 NPs[56] aqueous suspension arising from the CAN-mediated high-power ultrasonication (Sonics, Vibra cell, 750 W, power modulator setup at 25% with a Titanium horn for 30 min, 0 °C, dry inert argon atmosphere), 1 mL, Fe: 3.88 mg/mL − 3.88 mg total Fe, 0.0696 mmol Fe, ICP measurement) was diluted to 28.0 mL using Milli-Q purified H_2O. Then, 25.697 mg of 25 kDa *b*-PEI (0.001 mmol; PEI/Fe weight ratio, 6.7) was added to the NP suspension as an aqueous solution (10.0 mg of PEI/mL), the medium was then shaken for 48 h at 15 °C (orbital shaker−incubator). At the completion of such a mild PEI contacting/NP surface decoration, the resulting crude DoE-optimized $_{con}PEI_{25}$-CAN-γ-Fe_2O_3 NPs were washed 3 times (3 × 10 mL of ddH_2O) using an Amicon Ultra-15 centrifugal filter device (100 K) operated at 4000 rpm (12 min), followed by a size exclusion process performed using centrifugation (8000 rpm/min, 16 min, 18 °C and 7000 rpm, 10 min, 18 °C) to afford cleaned DoE-optimized $_{con}PEI_{25}$-CAN-γ-Fe_2O_3 NPs (using a PEI/Fe weight ratio of 6.7).

4.8. Nanocarrier Functionalization Using Various siRNA Species for Delivery/Gene Silencing. These experiments were performed in the same manner as described in the Supporting Information and in the reference Israel et al.[56] The following oligonucleotide sequences (sense/antisense) were used: 5′-GGACAU-CACCUAUGCCGAGUACUTC-3′/5′- ACCUGUAGUG-GAUACGGCUCAUGAAG-3′ (IDT Technologies).

4.9. Selected Procedures for Nanocarrier Functionalization Using Various siRNA Species for Delivery/Gene Silencing. *4.9.1. siRNA Adsorption (Gel Retardation Assay).* NP suspensions were diluted in water at different concentrations to reach different Fe/siRNA w/w ratios (0.063, 0.126, 0.315, 0.63, 0.945, and 1.26). To each NP suspension and control tube (C) (absence of particles), 2 μg of *Firefly* luciferase siRNA was added and incubated for 15 min at RT for a complex formation. After 15 min of incubation, the suspensions were loaded into 1.5% agarose gel that was prestained with ethidium bromide. The samples were electrophoresed at 100 mA for 30 min in a Tris-acetate (TAE) running buffer, and the bands were visualized using a UV imaging system (MiniLumi, DNR Bio-Imaging Systems Ltd.; the data are representative of the three independent experiments).

4.9.2. Cell Lines and Culture. U2OS human osteosarcoma cells were obtained from the American Type Culture Collection (ATCC). U2OS cells were cultured in Dulbecco's modified eagle medium (DMEM) supplemented with a 10% fetal bovine serum, 100 μg/mL penicillin, 100 U/mL streptomycin, and 2 mM L-glutamine (Biological Industries Ltd., Kibbutz Beit-Haemek, Israel). The dual luciferase-expressing U2OS cell line (U2OS-Luc) was generated as previously described.[69] All cells were grown at 37 °C in 5% CO_2.

4.9.3. Luciferase Assay. U2OS-Luc cells were seeded (1×10^4 cells/well) in a 96-well optical bottom plate (Thermo) and incubated overnight at 37 °C with 5% CO_2. U2OS-Luc cells were transfected with *Firefly* luciferase siRNA (0.166 μg; 100 nM) mixed with different types of NPs at different Fe/siRNA w/w ratios, or different siRNA concentrations, or without NPs (control). After 48 h, the cells were assayed for both *Firefly* and *Renilla* luciferase activities using the Dual Luciferase Assay System (Promega). Briefly, the cells were lysed and the *Firefly* luciferase substrate was added (50 μL/well dual substrate/buffer). The *Firefly* luciferase activity was measured after 10 min using a luminometer (Synergy 4, Biotek). Next, the *Renilla* luciferase substrate was added (50 μL/well Stop & GLO substrate/buffer) and the luminescence was measured after a further incubation of 10 min. The silencing efficacy was reflected by the luciferase activities that were normalized to control the luciferase activities.

4.9.4. Statistical Analysis. Statistical analysis of the data was performed with a GraphPad Prism software (GraphPad Software).

4.9.5. In Vivo Experiments. All animal experiments were performed in compliance with the Guidelines for the Care and Use of Research Animals established by the Bar-Ilan University Animal Studies Committee. BALB/c mice (Harlan Laboratories Israel Ltd., Jerusalem, Israel) aged 8−9 weeks were intravenously injected with NPs mixed with different doses of siRNA and different Fe/siRNA w/w ratios or saline alone. All intravenous injections to the mice were performed with RAC1 siRNA (sequence used only for the toxicity screening) provided by Quark Pharmaceuticals Inc., Ness Ziona, Israel. Each group was comprised of six mice. The acute toxicity was assessed as a mortality incidence post NP injection.

■ ASSOCIATED CONTENT

Ⓢ Supporting Information

Figures showing additional $_{con}PEI_{25}$-CAN-γ-Fe_2O_3 NCs-relating characterization data, SQUID, TEM, XPS, FTIR, and compositional EDAX analyses, observed siRNA adsorption and luciferase silencing data as well as one significant DoE optimization plot, FTIR spectra of starting neat *b*-PEI_{25} and oxidized *b*-PEI_{25} phases, and TEM and FTIR data for $_{con}PEI_{25}$-Hy-CAN-γ-Fe_2O_3 and $_{con}PEI_{25}$-Al-CAN-γ-Fe_2O_3 functional nanosystems. The Supporting Information is available free of charge on the ACS Publications website at DOI: 10.1021/acsami.5b02743.

■ AUTHOR INFORMATION

Corresponding Authors

*(J.-P.L.) E-mail: jean-paul.m.lellouche@biu.ac.il.
*(S.M.) E-mail: Shulamit.Michaeli@biu.ac.il.

Author Contributions

‖L.L.I. and E.L. equally contributed to this work.

Notes

The authors declare no competing financial interest.

■ ACKNOWLEDGMENTS

The funding by The 7th Framework RTD European Project (FP7-NMP-2010-LARGE-4 Area)—Large Collaborative Projects—Project SaveMe (Grant Agreement No. 263307), the Israel Ministry of Industry & Trade (Magnet "RIMONIM"), and the Israel Ministry of Industry & Trade (Project "KAMIN") is warmly acknowledged.

■ ABBREVIATIONS

Al, alginic acid
CAN, ceric ammonium nitrate
DLS, dynamic light scattering

DOI: 10.1021/acsami.5b02743
ACS Appl. Mater. Interfaces 2015, 7, 15240−15255

EA, elemental analysis
EDAX or EDS, energy-dispersive X-ray spectroscopy
EPR, enhanced permeability and retention effect
FTIR, Fourier transformation infrared spectroscopy
Hy, hyaluronic acid
iv, intravenous
LbL, layer-by-layer
NC(s), nanocarrier(s)
NP(s), nanoparticle(s)
PDMA, poly(*N*,*N*-dimethylacrylamide)
PEG, poly(ethylene glycol)
PEI, polyethylene imine
PLL, poly-L-lysine
PVA, poly(vinyl alcohol)
RBC, red blood cells
RISC, RNA-induced silencing complex
RT, room temperature
SQUID, superconducting quantum interference device
TEM, transmitting electron microscope
XPS, X-ray photoelectron spectroscopy
XRD, X-ray diffraction

REFERENCES

(1) Tartaj, P.; Morales, M. d. P.; Veintemillas-Verdaguer, S.; Gonzalez-Carreno, T.; Serna, C. J. The Preparation of Magnetic Nanoparticles for Applications in Biomedicine. *J. Phys. D: Appl. Phys.* **2003**, *36* (13), R182−R197.

(2) Wahajuddin; Arora, S. Superparamagnetic Iron Oxide Nanoparticles: Magnetic Nanoplatforms as Drug Carriers. *Int. J. Nanomed.* **2012**, *7*, 3445−3471.

(3) Amstad, E.; Textor, M.; Reimhult, E. Stabilization and Functionalization of Iron Oxide Nanoparticles for Biomedical Applications. *Nanoscale* **2011**, *3* (7), 2819−2843.

(4) Hilger, I.; Kaiser, W. A. Iron Oxide-Based Nanostructures for MRI and Magnetic Hyperthermia. *Nanomedicine (London, U. K.)* **2012**, *7* (9), 1443−1459.

(5) Ho, D.; Sun, X.-L.; Sun, S.-H. Monodisperse Magnetic Nanoparticles for Theranostic Applications. *Acc. Chem. Res.* **2011**, *44* (10), 875−882.

(6) Rosen, J. E.; Chan, L.; Shieh, D.-B.; Gu, F. X. Iron Oxide Nanoparticles for Targeted Cancer Imaging and Diagnostics. *Nanomedicine (N. Y., NY, U. S.)* **2012**, *8* (3), 275−290.

(7) Rümenapp, C.; Gleich, B.; Haase, A. Magnetic Nanoparticles in Magnetic Resonance Imaging and Diagnostics. *Pharm. Res.* **2012**, *29* (5), 1165−1179.

(8) Yigit, M. V.; Moore, A.; Medarova, Z. Magnetic Nanoparticles for Cancer Diagnosis and Therapy. *Pharm. Res.* **2012**, *29* (5), 1180−1188.

(9) Israel, L. L.; Kovalenko, E. I.; Boyko, A. A.; Sapozhnikov, A. M.; Rosenberger, I.; Kreuter, J.; Passoni, L.; Lellouche, J.-P. Towards Hybrid Biocompatible Magnetic rHuman Serum Albumin-Based Nanoparticles: Use of Ultra-Small $(CeL_n)^{3/4+}$ Cation-Doped Maghemite Nanoparticles as Functional Shell. *Nanotechnology* **2015**, *26* (4), 045601.

(10) Xu, C.; Sun, S. New Forms of Superparamagnetic Nanoparticles for Biomedical Applications. *Adv. Drug Delivery Rev.* **2013**, *65* (5), 732−743.

(11) Wang, Y.-X. J. Superparamagnetic Iron Oxide Based MRI Contrast Agents: Current Status of Clinical Application. *Quant. Imaging. Med. Surg.* **2011**, *1* (1), 35−40.

(12) Meister, G.; Tuschl, T. Mechanisms of Gene Silencing by Double-Stranded RNA. *Nature* **2004**, *431* (7006), 343−349.

(13) Hannon, G. J.; Rossi, J. J. Unlocking the Potential of the Human Genome with RNA Interference. *Nature* **2004**, *431* (7006), 371−378.

(14) Brummelkamp, T. R.; Bernards, R.; Agami, R. A System for Stable Expression of Short Interfering RNAs in Mammalian Cells. *Science* **2002**, *296* (5567), 550−553.

(15) Kanasty, R.; Dorkin, J. R.; Vegas, A.; Anderson, D. Delivery Materials for siRNA Therapeutics. *Nat. Mater.* **2013**, *12* (11), 967−977.

(16) Davis, M. E. The First Targeted Delivery of siRNA in Humans via a Self-Assembling, Cyclodextrin Polymer-Based Nanoparticle: From Concept to Clinic. *Mol. Pharmaceutics* **2009**, *6* (3), 659−68.

(17) Bartlett, D. W.; Davis, M. E. Physicochemical and Biological Characterization of Targeted, Nucleic Acid-Containing Nanoparticles. *Bioconjugate Chem.* **2007**, *18* (2), 456−468.

(18) Hu-Lieskovan, S.; Heidel, J. D.; Bartlett, D. W.; Davis, M. E.; Triche, T. J. Sequence-Specific Knockdown of EWS-FLI1 by Targeted, Nonviral Delivery of Small Interfering RNA Inhibits Tumor Growth in a Murine Model of Metastatic Ewing's Sarcoma. *Cancer Res.* **2005**, *65* (19), 8984−8992.

(19) Bao, Y.; Jin, Y.; Chivukula, P.; Zhang, J.; Liu, Y.; Liu, J.; Clamme, J. P.; Mahato, R. I.; Ng, D.; Ying, W.; Wang, Y.; Yu, L. Effect of PEGylation on Biodistribution and Gene Silencing of siRNA/lipid Nanoparticle Complexes. *Pharm. Res.* **2013**, *30* (2), 342−351.

(20) Belliveau, N. M.; Huft, J.; Lin, P. J.; Chen, S.; Leung, A. K.; Leaver, T. J.; Wild, A. W.; Lee, J. B.; Taylor, R. J.; Tam, Y. K.; Hansen, C. L.; Cullis, P. R. Microfluidic Synthesis of Highly Potent Limit-Size Lipid Nanoparticles for In Vivo Delivery of siRNA. *Mol. Ther.–Nucleic Acids* **2012**, *1*, e37.

(21) Biswas, S.; Deshpande, P. P.; Navarro, G.; Dodwadkar, N. S.; Torchilin, V. P. Lipid Modified Triblock PAMAM-Based Nanocarriers for siRNA Drug Co-Delivery. *Biomaterials* **2013**, *34* (4), 1289−1301.

(22) Liu, J.; Gu, C.; Cabigas, E. B.; Pendergrass, K. D.; Brown, M. E.; Luo, Y.; Davis, M. E. Functionalized Dendrimer-Based Delivery of Angiotensin Type 1 Receptor siRNA for Preserving Cardiac Function Following Infarction. *Biomaterials* **2013**, *34* (14), 3729−3736.

(23) Boyer, C.; Teo, J.; Phillips, P.; Erlich, R. B.; Sagnella, S.; Sharbeen, G.; Dwarte, T.; Duong, H. T.; Goldstein, D.; Davis, T. P.; Kavallaris, M.; McCarroll, J. Effective Delivery of siRNA Into Cancer Cells and Tumors Using Well-Defined Biodegradable Cationic Star Polymers. *Mol. Pharmaceutics* **2013**, *10* (6), 2435−2444.

(24) Cho, H. Y.; Averick, S. E.; Paredes, E.; Wegner, K.; Averick, A.; Jurga, S.; Das, S. R.; Matyjaszewski, K. Star Polymers with a Cationic Core Prepared by ATRP for Cellular Nucleic Acids Delivery. *Biomacromolecules* **2013**, *14* (5), 1262−1267.

(25) Soutschek, J.; Akinc, A.; Bramlage, B.; Charisse, K.; Constien, R.; Donoghue, M.; Elbashir, S.; Geick, A.; Hadwiger, P.; Harborth, J.; John, M.; Kesavan, V.; Lavine, G.; Pandey, R. K.; Racie, T.; Rajeev, K. G.; Röhl, I.; Toudjarska, I.; Wang, G.; Wuschko, S.; Bumcrot, D.; Koteliansky, V.; Limmer, S.; Manoharan, M.; Vornlocher, H. P. Therapeutic Silencing of an Endogenous Gene by Systemic Administration of Modified siRNAs. *Nature* **2004**, *432* (7014), 173−178.

(26) Jeong, J. H.; Mok, H.; Oh, Y. K.; Park, T. G. siRNA Conjugate Delivery Systems. *Bioconjugate Chem.* **2009**, *20* (1), 5−14.

(27) Heinemann, D.; Schomaker, M.; Kalies, S.; Schieck, M.; Carlson, R.; Escobar, H. M.; Ripken, T.; Meyer, H.; Heisterkamp, A. Gold Nanoparticle Mediated Laser Transfection for Efficient siRNA Mediated Gene Knock Down. *PLoS One* **2013**, *8* (3), e58604.

(28) Buchman, Y. K.; Lellouche, E.; Zigdon, S.; Bechor, M.; Michaeli, S.; Lellouche, J. P. Silica Nanoparticles and Polyethyleneimine (PEI)-Mediated Functionalization: a New Method of PEI Covalent Attachment for siRNA Delivery Applications. *Bioconjugate Chem.* **2013**, *24* (12), 2076−2087.

(29) Siu, K. S.; Chen, D.; Zheng, X.; Zhang, X.; Johnston, N.; Liu, Y.; Yuan, K.; Koropatnick, J.; Gillies, E. R.; Min, W. P. Non-Covalently Functionalized Single-Walled Carbon Nanotube for Topical siRNA Delivery into Melanoma. *Biomaterials* **2014**, *35* (10), 3435−3442.

(30) Park, T. G.; Jeong, J. H.; Kim, S. W. Current Status of Polymeric Gene Delivery Systems. *Adv. Drug Delivery Rev.* **2006**, *58* (4), 467−486.

(31) Suh, J.; Paik, H.; Hwang, B. K. Ionization of Poly(ethylenimine) and Poly(allylamine) at Various pH's. *Bioorg. Chem.* **1994**, *22*, 318−327.

DOI: 10.1021/acsami.5b02743
ACS Appl. Mater. Interfaces 2015, 7, 15240−15255

(32) Behr, J.-P. The Proton Sponge: A Trick to Enter Cells the Viruses Did Not Exploit. *Chimia* **1997**, 34−36.
(33) Nel, A. E.; Mädler, L.; Velegol, D.; Xia, T.; Hoek, E. M.; Somasundaran, P.; Klaessig, F.; Castranova, V.; Thompson, M. Understanding Biophysicochemical Interactions at the Nano-Bio Interface. *Nat. Mater.* **2009**, *8* (7), 543−557.
(34) Li, C.; Zhong, D.; Zhang, Y.; Tuo, W.; Li, N.; Wang, Q.; Liu, Z.; Xue, W. The Effect of the Gene Carrier Material Polyethyleneimine on the Structure and Function of Human Red Blood Cells in Vitro. *J. Mater. Chem. B* **2013**, *1* (14), 1885−1893.
(35) Petersen, H.; Fechner, P. M.; Martin, A. L.; Kunath, K.; Stolnik, S.; Roberts, C. J.; Fischer, D.; Davies, M. C.; Kissel, T. Polyethylenimine-Graft-Poly(ethylene glycol) Copolymers: Influence of Copolymer Block Structure on DNA Complexation and Biological Activities as Gene Delivery System. *Bioconjugate Chem.* **2002**, *13* (4), 845−854.
(36) Höbel, S.; Aigner, A. Polyethylenimines for siRNA and miRNA Delivery in Vivo. *Wiley Interdiscip. Rev.: Nanomed. Nanobiotechnol.* **2013**, *5* (5), 484−501.
(37) Park, S. C.; Nam, J. P.; Kim, Y. M.; Kim, J. H.; Nah, J. W.; Jang, M. K. Branched Polyethylenimine-Grafted-Carboxymethyl Chitosan Copolymer Enhances the Delivery of pDNA or siRNA In Vitro and In Vivo. *Int. J. Nanomed.* **2013**, *8*, 3663−3677.
(38) Yang, X. C.; Niu, Y. L.; Zhao, N. N.; Mao, C.; Xu, F. J. A Biocleavable Pullulan-Based Vector via ATRP for Liver Cell-Targeting Gene Delivery. *Biomaterials* **2014**, *35* (12), 3873−3884.
(39) Jiang, G.; Park, K.; Kim, J.; Kim, K. S.; Hahn, S. K. Target Specific Intracellular Delivery of siRNA/PEI-HA Complex by Receptor Mediated Endocytosis. *Mol. Pharmaceutics* **2009**, *6* (3), 727−737.
(40) Gusachenko (Simonova), O.; Kravchuk, Y.; Konevets, D.; Silnikov, V.; Vlassov, V. V.; Zenkova, M. A. Transfection Efficiency of 25-kDa PEI-Cholesterol Conjugates with Different Levels of Modification. *J. Biomater. Sci., Polym. Ed.* **2009**, *20* (7−8), 1091−1110.
(41) Amjad, M. W.; Amin, M. C.; Katas, H.; Butt, A. M. Doxorubicin-Loaded Cholic Acid-Polyethyleneimine Micelles for Targeted Delivery of Antitumor Drugs: Synthesis, Characterization, and Evaluation of their In Vitro Cytotoxicity. *Nanoscale Res. Lett.* **2012**, *7* (1), 687.
(42) Hu, F. Q.; Chen, W. W.; Zhao, M. D.; Yuan, H.; Du, Y. Z. Effective Antitumor Gene Therapy Delivered by Polyethylenimine-Conjugated Stearic Acid-g-Chitosan Oligosaccharide Micelles. *Gene Ther.* **2013**, *20* (6), 597−606.
(43) Liu, Y. Y.; Yang, X. Y.; Li, Z.; Liu, Z. L.; Cheng, D.; Wang, Y.; Wen, X. J.; Hu, J. Y.; Liu, J.; Wang, L. M.; Wang, H. J. Characterization of Polyethylene Glycol-Polyethyleneimine as a Vector for Alpha-Synuclein siRNA Delivery to PC12 Cells for Parkinson's Disease. *CNS Neurosci. Ther.* **2014**, *20* (1), 76−85.
(44) Zhou, L.; Chen, Z.; Wang, F.; Yang, X.; Zhang, B. Multifunctional Triblock Co-Polymer mP3/4HB-b-PEG-b-lPEI for Efficient Intracellular siRNA Delivery and Gene Silencing. *Acta Biomater.* **2013**, *9* (4), 6019−6031.
(45) Chen, Y.; Lian, G.; Liao, C.; Wang, W.; Zeng, L.; Qian, C.; Huang, K.; Shuai, X. Characterization of Polyethylene Glycol-Grafted Polyethylenimine and Superparamagnetic Iron Oxide Nanoparticles (PEG-g-PEI-SPION) as an MRI-Visible Vector for siRNA Delivery in Gastric Cancer in Vitro and in Vivo. *J. Gastroenterol.* **2013**, *48* (7), 809−821.
(46) Cole, A. J.; Yang, V. C.; David, A. E. Cancer Theranostics: the Rise of Targeted Magnetic Nanoparticles. *Trends Biotechnol.* **2011**, *29* (7), 323−332.
(47) Petri-Fink, A.; Hofmann, H. Superparamagnetic Iron Oxide Nanoparticles (SPIONs): From Synthesis to In Vivo Studies - A Summary of the Synthesis, Characterization, In Vitro, and In Vivo Investigations of SPIONs with Particular Focus on Surface and Colloidal Properties. *IEEE Trans Nanobioscience* **2007**, *6* (4), 289−297.
(48) Davis, M. E.; Zuckerman, J. E.; Choi, C. H. J.; Seligson, D.; Tolcher, A.; Alabi, C. A.; Yen, Y.; Heidel, J. D.; Ribas, A. Evidence of RNAi in Humans from Systemically Administered siRNA via Targeted Nanoparticles. *Nature* **2010**, *464* (7291), 1067−1070.
(49) Whitehead, K. A.; Langer, R.; Anderson, D. G. Knocking Down Barriers: Advances in siRNA Delivery. *Nat. Rev. Drug Discovery* **2009**, *8* (2), 129−138.
(50) Yuan, X.; Naguib, S.; Wu, Z. Recent Advances of siRNA Delivery by Nanoparticles. *Expert Opin. Drug Delivery* **2011**, *8* (4), 521−536.
(51) Higuchi, Y.; Kawakami, S.; Hashida, M. Strategies for In Vivo Delivery of siRNAs. *BioDrugs* **2010**, *24* (3), 195−205.
(52) Haviv, A. H.; Grenèche, J.-M.; Lellouche, J.-P. Aggregation Control of Hydrophilic Maghemite (γ-Fe_2O_3) Nanoparticles by Surface Doping Using Cerium Atoms. *J. Am. Chem. Soc.* **2010**, *132* (36), 12519−12521.
(53) Deleersnyder, K.; Schaltin, S.; Fransaer, J.; Binnemans, K.; Parac-Vogt, T. N. Ceric Ammonium Nitrate (CAN) as Oxidizing or Nitrating Reagent for Organic Reactions in Ionic Liquids. *Tetrahedron Lett.* **2009**, *50* (32), 4582−4586.
(54) Dhakshinamoorthy, A.; Pitchumani, K. Clay-Supported Ceric Ammonium Nitrate as an Effective, Viable Catalyst in the Oxidation of Olefins, Chalcones and Sulfides by Molecular Oxygen. *Catal. Commun.* **2009**, *10* (6), 872−878.
(55) Isiklan, N.; Kursun, F.; Inal, M. Graft Copolymerization of Itaconic Acid onto Sodium Alginate Using Ceric Ammonium Nitrate as Initiator. *J. Appl. Polym. Sci.* **2009**, *114* (1), 40−48.
(56) Israel, L. L.; Lellouche, E.; Kenett, R.; Green, O.; Michaeli, S.; Lellouche, J. P. $Ce^{3/4+}$ Cation-Functionalized Maghemite Nanoparticles Towards siRNA-Mediated Gene Silencing. *J. Mater. Chem. B* **2014**, *2* (37), 6215−6225.
(57) Lellouche, J.-P.; Michaeli, S.; Israel, L. L.; Lellouche, E.; Kapilov-Buchman, Y. Magnetic Inorganic Iron-Based Nanoparticles. Generalities and Use in Drug Delivery. PCT International Patent Application, WO 2014147608 A120140925, Jan. 19, 2014.
(58) Massart, R.; Dubois, E.; Cabuil, V.; Hasmonay, E. Preparation and Properties of Monodisperse Magnetic Fluids. *J. Magn. Magn. Mater.* **1995**, *149* (1), 1−5.
(59) Karraker, D. G. Coordination of Trivalent Lathanide Ions. *J. Chem. Educ.* **1970**, *47* (6), 424−430.
(60) Limaye, S. N.; Saxena, M. C. Relative Complexing Tendencies of Oxygen-Oxygen, Oxygen-Nitrogen, and Oxygen-Sulfur Donor (Secondary) Ligands in Some Lanthanide-EDTA Mixed-Ligand Complexes. *Can. J. Chem.* **1986**, *64* (5), 865−870.
(61) Arnold, P. L.; Casely, I. J.; Zlatogorsky, S.; Wilson, C. Organometallic Cerium Complexes from Tetravalent Coordination Complexes. *Helv. Chim. Acta* **2009**, *92* (11), 2291−2303.
(62) Aghabozorg, H.; Roshan, L.; Firoozi, N.; Bagheri, S.; Ghorbani, Z.; Kalami, S.; Mirzaei, M.; Shokrollahi, A.; Ghaedi, M.; Aghaei, R.; Ghadermazi, M. Syntheses, Crystal, and Molecular Structures of Mn(II), Zn(II), and Ce(III) Compounds and Solution Studies of Mn(II), Ni(II), Cu(II), Zn(II), Cd(II), and Ce(III) Compounds Obtained from a Suitable Proton Transfer Compound Containing bda and pydcH2 (bda = butane-1,4-diamine; pydcH2 = pyridine-2,6-dicarboxylic acid). *Struct. Chem.* **2010**, *21* (4), 701−714.
(63) Edelmann, F. T. Lanthanides and Actinides: Annual Survey of Their Organometallic Chemistry Covering the Year 2009. *Coord. Chem. Rev.* **2012**, *256* (11−12), 1151−1228.
(64) Zintchenko, A.; Philipp, A.; Dehshahri, A.; Wagner, E. Simple Modifications of Branched PEI Lead to Highly Efficient siRNA Carriers with Low Toxicity. *Bioconjugate Chem.* **2008**, *19* (7), 1448−1455.
(65) Mao, S.; Neu, M.; Germershaus, O.; Merkel, O.; Sitterberg, J.; Bakowsky, U.; Kissel, T. Influence of Polyethylene Glycol Chain Length on the Physicochemical and Biological Properties of Poly(ethyleneimine)-graft-Poly(ethylene glycol) Block Copolymer/SiRNA Polyplexes. *Bioconjugate Chem.* **2006**, *17* (5), 1209−121866.
(66) Seow, W. Y.; Liang, K.; Kurisawa, M.; Hauser, C. A. Oxidation as a Facile Strategy to Reduce the Surface Charge and Toxicity of Polyethyleneimine Gene Carriers. *Biomacromolecules* **2013**, *14* (7), 2340−2346.

DOI: 10.1021/acsami.5b02743
ACS Appl. Mater. Interfaces 2015, 7, 15240−15255

(67) Sarin, V. K.; Kent, S. B. H.; Tam, J. P.; Merrifield, R. B. Quantitative Monitoring of Solid-Phase Peptide-Synthesis by the Ninhydrin Reaction. *Anal. Biochem.* **1981**, *117* (1), 147−157.
(68) Arnold, P. L.; Casely, I. J.; Zlatogorsky, S.; Wilson, C. Organometallic Cerium Complexes from Tetravalent Coordination Complexes. *Helv. Chim. Acta* **2009**, *92* (11), 2291−2303.
(69) Buchman, Y. K.; Lellouche, E.; Zigdon, S.; Bechor, M.; Michaeli, S.; Lellouche, J.-P. Silica Nanoparticles and Polyethyleneimine (PEI)-Mediated Functionalization: A New Method of PEI Covalent Attachment for siRNA Delivery Applications. *Bioconjugate Chem.* **2013**, *24* (12), 2076−2087.

DOI: 10.1021/acsami.5b02743
ACS Appl. Mater. Interfaces 2015, 7, 15240−15255